A DIGITAL COMPUTER STUDY OF THE
FIRST-STAGE TRAJECTORIES OF HIGH
INITIAL ACCELERATION ROCKETS

GORDON HOWLAND JAYNE
and
JOSEPH BARBOUR WILKINSON, JR.

A DIGITAL COMPUTER STUDY OF THE FIRST-STAGE

TRAJECTORIES OF HIGH INITIAL ACCELERATION ROCKETS

by

Lieutenant Gordon Howland Jayne, U.S. Navy
B.S., U.S. Naval Academy, 1952
B.S., Aero. Eng., U.S. Naval Postgraduate School, 1960

and

Lieutenant Joseph Barbour Wilkinson, Jr., U.S. Navy
B.S., U.S. Naval Academy, 1952
B.S., Aero. Eng., U.S. Naval Postgraduate School, 1960

Submitted in Partial Fulfillment
of the Requirements for the
Degree of Master of Science

at the

MASSACHUSETTS INSTITUTE OF TECHNOLOGY
June 1961

A DIGITAL COMPUTER STUDY OF THE FIRST-STAGE
TRAJECTORIES OF HIGH INITIAL ACCELERATION ROCKETS

by

Gordon H. Jayne

and

Joseph B. Wilkinson, Jr.

ABSTRACT

The first-stage, powered-flight trajectory of a large rocket powered vehicle is studied by varying the initial acceleration, the vertical flight time, and the initial tilt angle. Trajectories were computed on an IBM 650 digital computer. Specific areas of interest with respect to high initial acceleration rockets are the feasibility of using the "gravity turn" maneuver to obtain low burnout flight path angles, and the determination of maximum energy trajectories for various values of initial acceleration.

Results indicate that a relatively low initial tilt angle followed by a "gravity turn" maneuver is not adequate to achieve low burnout flight path angles for high initial acceleration vehicles. For values of initial acceleration of about 2.5 to 3.0 a large percentage of burning time is spent in the programmed tilting phase, which results in lift load factors of the order of .8 to 1.2.

Maximum energy trajectories occur at specific values of burnout flight path angle for the initial accelerations considered. These burnout angles start at about fifty-five degrees for an initial acceleration of 3.0 and decrease to approximately zero degrees for an initial acceleration of 1.5.

Burnout conditions of velocity, altitude, energy, and flight path angle are plotted for the trajectories computed. The trajectories most closely approximating the maximum energy cases are included in tabular form.

ACKNOWLEDGEMENTS

The authors wish to express their appreciation to the following persons: Professor Paul E. Sandorff for his advice and guidance during this project, Mr. Lawrence J. Berman who supplied much background material and encouragement, and Miss Mary Carlo who typed the manuscript.

Acknowledgement is also made to Mr. Richard Russell, Mr. Hugh Blair-Smith, and Mrs. R. H. Walker of the Mathematics Group of the MIT Instrumentation Laboratory for their instruction in problem programming for the IBM-650 digital computer.

The graduate work for which this thesis is a partial requirement was performed while the authors were assigned from the U. S. Naval Postgraduate School for graduate training at the Massachusetts Institute of Technology.

TABLE OF CONTENTS

TABLE OF CONTENTS (Continued)

LIST OF SYMBOLS

A	Cross-sectional area, ft^2
c	Exhaust velocity, ft/sec
C_D	Drag coefficient
C_{D_O}	Zero-lift drag coefficient
C_{D_c}	Cross-flow drag coefficient
C_L	Lift coefficient
D	Drag force, lb
DT	Time interval, sec
E	Total energy, ft-lb/slug
E_b	Total energy at burnout, ft-lb/slug
F	Thrust, lb
g_{ave}	Average acceleration of gravity
g_o	Gravitational conversion factor, 32.17405 ft/sec^2
I_s	Specific thrust, sec
L	Lift, lb
M	Mach number
M_c	Cross-flow Mach number
MR	Mass ratio
m	Mass, slug
n_i	Initial thrust to weight ratio
n_L	Lift load factor
R	Density ratio, ρ/ρ_o
S	Planform area, ft^2

LIST OF SYMBOLS (Continued)

T	Time, sec
T_b	Burnout time, sec
T_u	Fictitious burnup time, sec
T_v	Vertical flight time, sec
U	Angle of missile axis from vertical, deg or rad
U_m	Maximum programmed U, deg or rad
V	Velocity, ft/sec
V_b	Velocity at burnout, ft/sec
V_D	Velocity loss due to drag force
V_G	Velocity loss due to gravity
V_s	Speed of sound, ft/sec
$\dot{w}$	Weight flow rate lb/sec
W_i	Initial weight, lb
X	Horizontal range, ft
Y	Altitude, ft
Y_b	Altitude of burnout, ft
α	Angle of attack, deg or rad
γ	Flight path angle, deg or rad
γ_b	Flight path angle at burnout, deg or rad
ρ	Atmospheric density, $slug/ft^2$
ρ_o	Atmospheric density at sea level, $slug/ft^3$

OBJECT

The object of this thesis is to study the early powered-flight trajectory of a large rocket powered vehicle. The effects on the first-stage trajectory of varying vertical flight time, initial tilt angle, and initial acceleration, are of primary interest, especially as they affect the maximum burnout energy conditions.

Of interest also is the feasibility of using a relatively small initial tilt angle followed by a "gravity turn" to reach practical burnout conditions of velocity, altitude, and flight path angles for vehicles with high initial acceleration.

CHAPTER 1

INTRODUCTION

The study reported herein is concerned primarily with the initial portions of the powered-flight trajectory of a large, single stage, rocket powered vehicle. Conceptually, this vehicle could be the booster stage of an ICBM or a satellite launcher.

Usually there are three phases to the initial flight trajectory of a large ballistic missile or satellite launching vehicle. These phases include a vertical flight phase, a tilt phase, and a gravity turn phase. The gravity turn phase is customarily followed by a period of "constant-attitude thrust", during which the major portion of the flight velocity is achieved; this latter regime is not considered in this study.

A vertical launch for a large, rocket-powered vehicle of current design is necessary due to the inability of the vehicle structurally to withstand the transverse loads which would be present during an inclined launch. Vertical or near vertical flight is also necessary in order to achieve altitude. Usually the vertical flight path is followed for a short time, but the time of vertical flight must be carefully selected in order to achieve a trajectory which minimizes propellant expenditure.

Upon completion of the vertical flight phase, a tilting phase is commenced. Tilting is normally accomplished by deflecting the thrust vector of the vehicle to produce a tilting moment according to some selected program;

this changes the attitude of the vehicle, and subsequent thrusting changes the velocity vector. This maneuver is non-optimum and is best completed quickly; however, the tilt rate must not be so rapid as to exceed practical limitations of the vehicle control and structure. The tilting phase is completed when the vehicle body axis and the thrust vector are both aligned with the vehicle velocity vector.

The third phase of the conventional trajectory concerns the flight regime where this alignment exists and a relatively slow turning path follows, brought about by the component of gravity transverse to the flight path. This phase hopefully terminates at an altitude above the sensible atmosphere, and with an attitude that matches the subsequent constant-attitude thrust regime in such a manner that the best overall trajectory performance is obtained.

The important problem of proceeding from the earth's surface, through the three phases of the trajectory outlined, to arrive at a desirable altitude, velocity and attitude, is complicated because of the external forces acting on the vehicle. The major forces affecting the vehicle during these phases are thrust, the earth's gravitational force, and the aerodynamic forces of lift and drag, which act in a direction perpendicular and parallel to the instantaneous direction of flight, respectively. Gravitational and drag forces acting on the vehicle result in velocity losses during the flight and thus detract from the efficiency of the launch. The lift force may in certain cases be beneficial in that it may aid in turning the vehicle.

For a specific vehicle, the important trajectory design parameters are velocity, altitude, and flight path angle at burnout. It is only possible however, to compute trajectory characteristics by numerical integration of the equations of motion from specified initial conditions. In this paper numerous

trajectories are developed, using vehicle characteristics which are approx-
imately representative of large chemical rockets of contemporary design, and
varying the time of vertical flight and the maximum tilt angle. The effects
of variations in two important vehicle design parameters are also included:
namely, the initial thrust-to-weight ratio, n_i, and the mass ratio; the value
of n_i is introduced as an additional initial variable, while with the assump-
tion of constant mass flow every point in each computed trajectory corresponds
to burnout for some specific mass ratio. The burnout conditions are then
examined as functions of the initial variables by using burnout angle as a
governing parameter and cross-plotting. The nature of trajectory optimization
to maximize burnout velocity or burnout energy is of particular concern to
this study.

CHAPTER 2

VEHICLE DESCRIPTION AND AERODYNAMICS

This study is intended to derive conclusions applicable to rocket vehicles similar to contemporary long range ballistic missiles, satellite launchers, and space vehicle boosters. Development of trajectory data requires the use of certain vehicle design parameters which identify aerodynamic and engine performance. To simplify preliminary work the "high-drag" configuration missile of Ref. 1 is selected as a model. It is believed that this design has aerodynamic characteristics representative of the class of vehicles described above. Rocket engine specific impulse is taken to be 300 lb-sec/lb, and, again for simplification, this value is considered constant throughout the flight regime. A value of 10 is selected for the ratio of initial weight to burnout weight, defined as the mass ratio. This makes the propellant factor, the ratio of initial fuel weight to initial vehicle weight, equal to .9. Figure 1 shows the physical dimensions of the selected vehicle.

Since the vehicle of this study is similar to the high drag missile of Ref. 1, the aerodynamic coefficients utilized are extracted from this source. A detailed explanation of the methods and procedures used to arrive at these values are set forth in Appendix G of that report.

The missile, being axially-symmetric, has only a drag force imposed on it during the vertical flight phase and the gravity turn phase, since
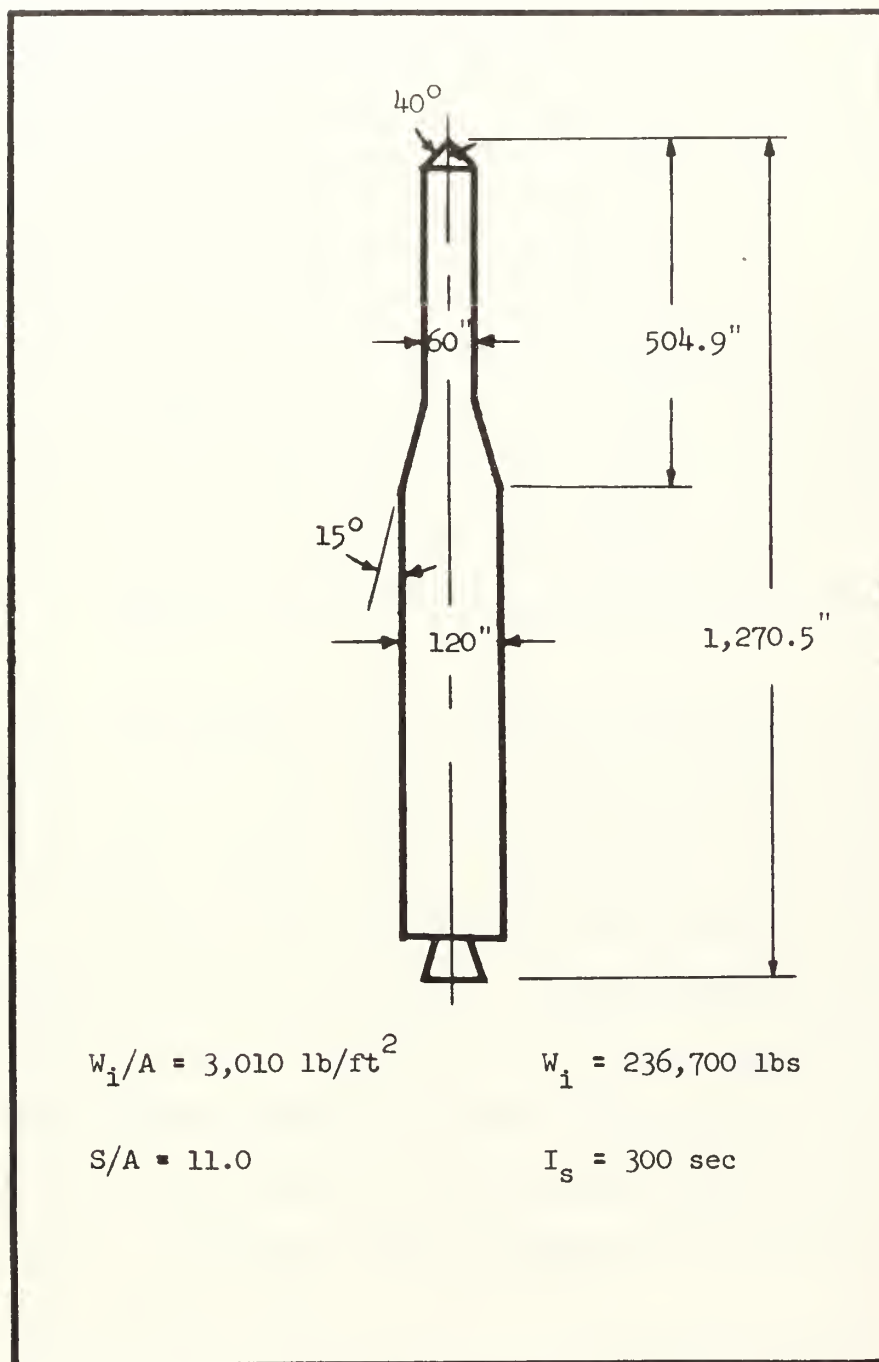
Fig. 1   Missile configuration.   (Reference 1)

during these phases the angle-of-attack is zero. The zero-lift drag force is made up of three parts: base drag, skin friction drag, and form drag. The zero-lift drag coefficient, based upon both theoretical and empirical data, and representing the sum of these forces, is plotted versus Mach number in Fig. 2.

In order to simplify computer programming, the curve of C_{D_O} versus Mach number is divided into five segments. Each segment of the curve is then represented by a straight line function. The breakdown of the C_{D_O} curve and the approximating straight line functions are shown in Table I. This straight line approximation of the curve representing C_{D_O}, while being an approximation, is considered to be sufficiently accurate for the problem at hand.

During the tilting phase of the trajectory, the missile is subjected to lift forces, as well as drag forces, since the missile has an angle of attack during transition from the vertical flight phase to the zero-lift phase. Reference 1 outlines a cross-flow method of predicting lift and drag on bodies of revolution at an angle of attack. In this method the flow over the missile is separated into two components: one along the axial direction of the body, and one component normal to the axis. The axial flow exerts a force on the body in the axial direction while the cross flow exerts a force in the normal direction. Reference 1 derives equations for C_L and C_D using this theory of cross and axial flow.

$$C_L = (2 - C_{D_O})\alpha + (S/A) \, C_{D_c}\alpha^2$$

$$C_D = C_{D_O} - (1 - C_{D_O})\alpha^2 + \alpha C_L$$
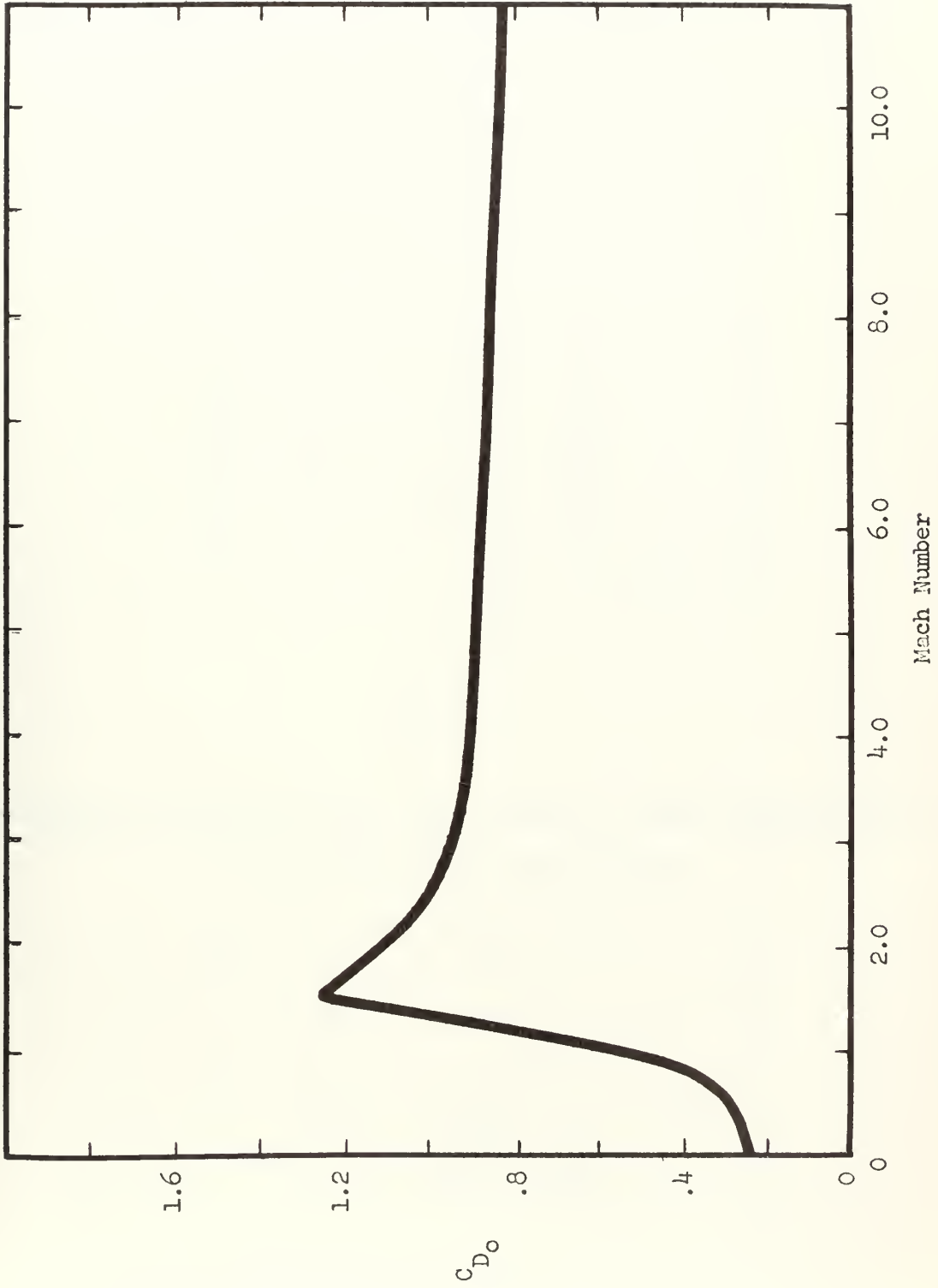
Fig. 2 Zero-lift drag coefficient for two cone-cylinder bodies. (Reference 1)

TABLE I

STRAIGHT LINE APPROXIMATIONS OF THE ZERO-LIFT DRAG COEFFICIENT CURVE

FOR VARIOUS VALUES OF MACH NUMBER

M	C_{D_c}
0	
	.130
0.72	
	.850M - .482
1.25	
	.983 - .323M
1.90	
	.522 - .080M
3.4	
	.328 - .023M
7.3	
	.155

TABLE II

STRAIGHT LINE APPROXIMATIONS OF THE CROSS-FLOW DRAG COEFFICIENT CURVE

FOR VARIOUS VALUES OF MACH NUMBER

M	C_{D_c}
0	
	.80
.4	
	$3.23M_c - .49$
.75	
	$2.36 - .573M_c$

The term C_{D_C} is a drag coefficient due to the cross flow component. A plot
of C_{D_C} versus Mach number, assumed to apply for this study, is shown in
Fig. 3. This plot is a series of straight line approximations of the cross-
flow drag characteristics derived in Ref. 1 for the missile configuration of
Fig. 1. These straight line approximations are described by functions as
set forth in Table II. The straight line approximations are considered
sufficiently accurate since, as it can be seen from the above equation, the
effect of C_{D_C} is minor at small angles of attack.
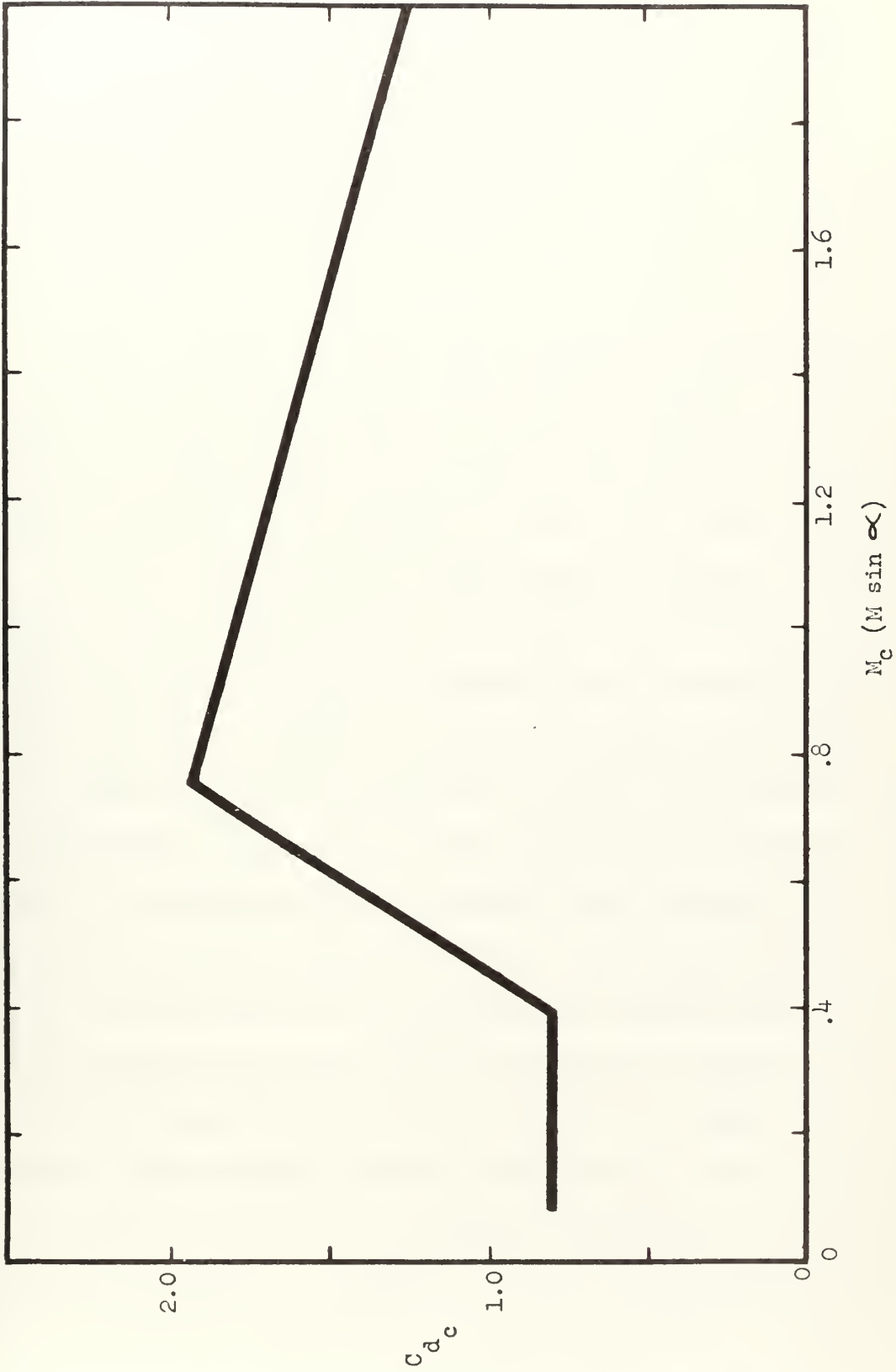
Fig. 3 Cross-flow drag coefficient versus cross-flow Mach number. (Reference 1)

CHAPTER 3

TRAJECTORY ANALYSIS

The portion of the powered flight trajectory of interest in this study is considered in three phases, as discussed in Chapter 1. The first phase or vertical flight regime is followed by the tilt phase during which the vehicle is tilted from the vertical at a rate of two degrees per second.

In Ref. 1 the tilt phase is approximated by impulsive tilting to 5.5 degrees from the vertical during a one second time interval at the end of vertical flight time, followed by a gravity turn which continues until the desired conditions of attitude, altitude, and velocity are reached. The vehicle is assumed to be in the gravity turn as soon as the impulsive tilting is accomplished. The impulsive tilting during a one second time interval is justified by determining that the required vehicle response time is less than one second for the 5.5 degree tilt angle. This computation is made on the basis of the time required to tilt through the specified angle with the maximum tilting moment available acting on the moment of inertia of the vehicle. For the present study, which is concerned with higher values of n_i and consequent higher dynamic pressures during tilting, a tilt rate of 2 degrees per second is selected as a reasonable maximum value. This is perhaps lower than necessary for tilting at sea level, but to have a basis for comparison, this rate is used for all trajectories computed. In the computer this tilt rate is approximated by increasing the tilt angle, U, two degrees

per second until the tilt angle reaches the specified maximum programmed tilt angle, U_m. This value of tilt angle is then held constant until the angle-of-attack of the missile becomes zero. At this time the tilt phase ends and the zero angle-of-attack or gravity turn phase begins. During the tilt phase thrust is considered to act parallel to the vehicle axis. The component of thrust required for tilt is considered a negligible loss compared to the total thrust vector.

In the zero angle-of-attack phase thrust acts in the direction of the instantaneous velocity vector, which is also parallel to the missile axis. Turning is accomplished by the action of the earth's gravitational field. This part of the trajectory would logically be followed by a constant attitude or a "linear with time" thrust program, depending on the mission of the vehicle. In this study the gravity turn is continued until ninety percent of the missile mass is consumed. Since this paper deals only with single stage characteristics, staging is not considered and all results pertain to first-stage values.

CHAPTER 4

EQUATIONS OF MOTION

The equations of motion are developed using an inertial X, Y coordinate frame. This assumes a "flat", non-rotating earth, which is a good approximation during the early powered-flight phase of the type of rocket vehicle considered. The gravitational acceleration due to the earth is assumed to be constant during the portion of the trajectory of interest in this paper. This also is a reasonable assumption when the altitude reached is small compared with the radius of the earth, as it is in this study.

Rocket engine characteristics are simplified by assuming constant thrust and constant mass flow rate. Both of these quantities usually vary with atmospheric pressure, thrust increasing and mass flow rate decreasing as altitude is increased. This means that the specific impulse actually increases with altitude and that the initial thrust-to-weight ratio is based on the lower level of thrust found at sea level. The simplifications made in this study specify a constant specific impulse of 300 seconds, which may be thought of as representing an average value. The initial thrust-to-weight ratio in this study is therefore somewhat larger than it would be for an actual vehicle of comparable performance.

Considering the vehicle as a point mass the equations of motion are

$$D^2Y/DT^2 = (F/m)\cos U - g_{ave} - (D/m)\sin \gamma - (L/m)\cos \gamma \qquad (1)$$

$$D^2X/DT^2 = (F/m)\sin U - (D/m)\cos \gamma + (L/m)\sin \gamma \qquad (2)$$

wherein

F/m = thrust per unit mass

g_{ave} = gravitational acceleration due to the earth

D/m = drag per unit mass

L/m = lift per unit mass

The lift terms are considered positive in sign for the negative angle-of-attack condition which occurs during the tilt phase of the trajectory. Figure 4 shows the vector relationships involved.

Thrust, lift, and drag forces per unit mass are computed using the nomenclature of Ref. 2, in which T_u is defined as a fictitious time when the total mass of the vehicle would be consumed.

$$T_u = W_i/\dot{w} = I_s/n_i \qquad (3)$$

From the conventional relationships between rocket parameters

$$I_s = F/\dot{w} \qquad (4)$$

$$m = W_i/g_o(1 - T/T_u) \qquad (5)$$

$$c = I_s g_o \qquad (6)$$

Applying (4), (5), and (6) to the various accelerations due to thrust, lift, and drag in (1) and (2) gives

$$F/m = c/(T_u - T) \qquad (7)$$
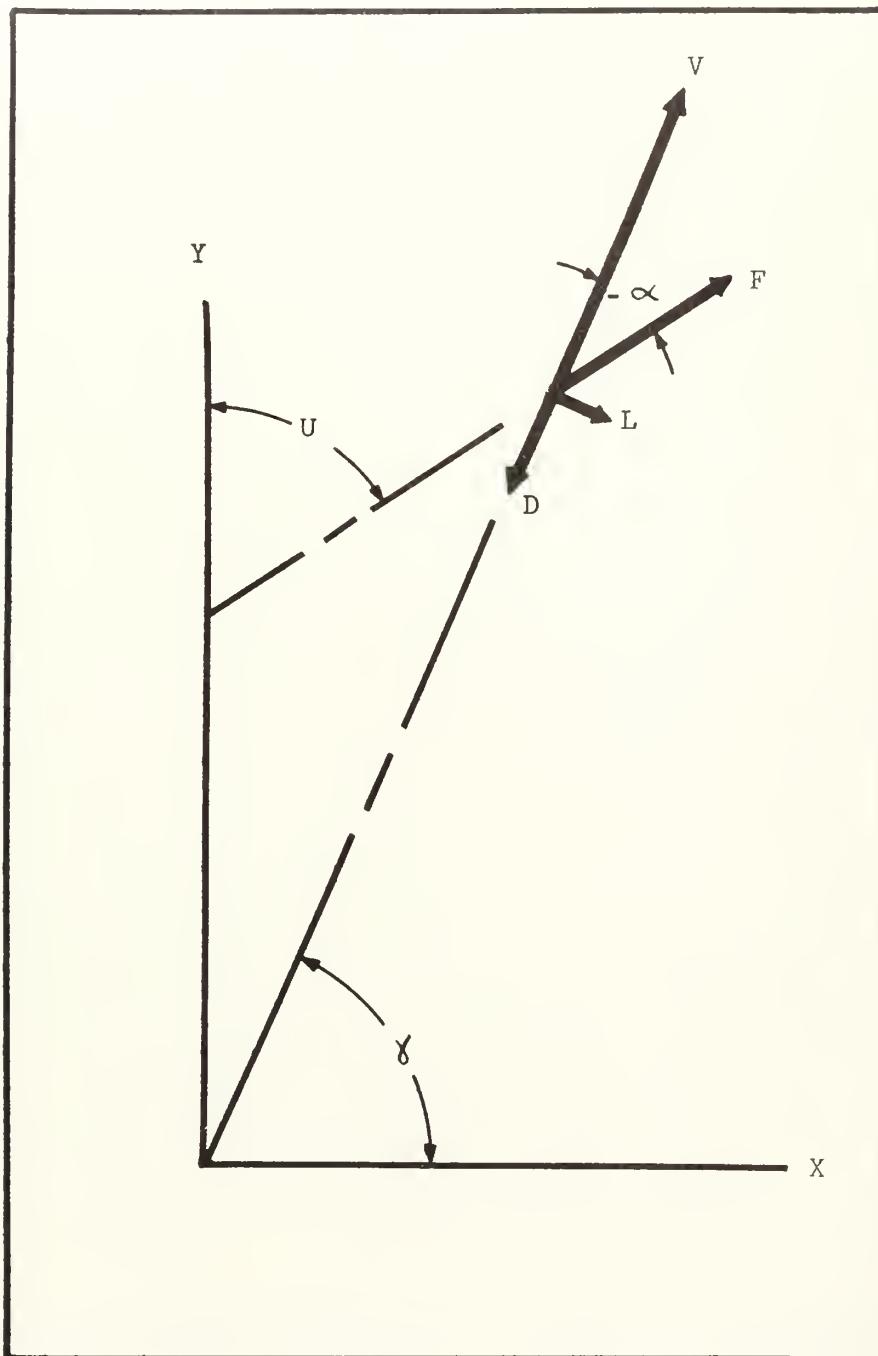
Fig. 4   Simplified diagram of vector quantities associated with the missile.

$$D/m = (\tfrac{1}{2}\rho V^2 C_D A g_o T_u)/W_i(T_u-T) \qquad\qquad (8)$$

$$L/m = (\tfrac{1}{2}\rho V^2 C_L A g_o T_u)/W_i(T_u-T) \qquad\qquad (9)$$

CHAPTER 5

COMPUTER PROGRAM

The computer used in this study is an IBM 650 digital computer located in the computation center of the Instrumentation Laboratory of the Massachusetts Institute of Technology. Although not comparable in speed to the larger digital computers such as the IBM 704, it is adequate for this study, computing an average trajectory in about ten minutes. The computer program is prepared using the MAC programming system developed by the Instrumentation Laboratory computation center.

Time intervals for integration are varied according to the phase of the trajectory. During the vertical flight phase the time interval is set at four seconds for vertical flight times of four seconds and above, and one second for vertical flight times less than four seconds. The time interval is reduced to one second during the tilt phase to maintain comparable accuracy in computing the rapidly changing trajectory quantities. At the completion of the tilt phase the time interval is increased again to four seconds and is held constant until burnout.

The initial conditions for the equations of motion are set equal to zero for each run. Parameters held constant for all runs are: S/A, W_i/A, DU/DT, I_s, and $\dot{w}$. Variable parameters for each run are: T_v, T_u, and U_m. The fictitious burn-up time, T_u, equals I_s/n_i. Since I_s is held constant, T_u is directly proportional to n_i. Table III lists the numerical values of the constants and parameters used.

TABLE III

NUMERICAL VALUES OF CONSTANTS AND PARAMETERS

Symbol	Value	Description
ρ_o	.0023769 slug/ft^3	Atmospheric density at sea level
g_o	32.17405 ft/sec^2	Gravitational conversion factor
g_{ave}	32.0 ft/sec^2	Gravitational acceleration acting on vehicle (assumed constant)
S/A	11.0	Ratio of planform area to cross section area
W_i/A	3010 lb/ft^2	Ratio of initial weight to cross section area
DU/DT	2 deg/sec	Tilt rate
I_s	300 sec	Average specific impulse

n_i	T_u sec	T_b sec
3.0	100	90
2.5	120	108
2.0	150	135
1.5	200	180

Tilt rate is held constant at two degrees per second until U_m is reached. This is mechanized on the computer by increasing U instantaneously at the beginning of each one second time interval until U equals U_m. At this point U_m is held constant until the angle of attack becomes zero. Lift and drag are computed during the tilt phase in the manner shown in Chapters 2 and 4. These calculations are made at the beginning of each time interval and are integrated as constants within the differential equation loop of the program. The error introduced by this approximation was small, as a result of the selection of integration intervals; in general the change in aerodynamic force from one interval to the next did not exceed three percent. When the angle-of-attack becomes zero, U is set equal to $(90^\circ - \gamma)$, and thereafter varies directly with γ. This point marks the beginning of the gravity turn phase.

In the gravity turn phase lift is set equal to zero and drag is calculated in the same manner as above using the zero angle-of-attack drag coefficient. The program is terminated when T equals .9 T_u, which corresponds to the mass ratio of ten mentioned in Chapter 2. Values of velocity, altitude, range, flight path angle, and energy are punched for each computer time interval, and for burnout.

CHAPTER 6

RESULTS

For the study and results as presented here, all vehicle and
trajectory parameters are held constant, except the initial thrust-to-
weight ratio of the vehicle, the time of vertical flight, and the maxi-
mum programmed tilt angle. The initial thrust-to-weight ratios used are
1.5, 2.0, 2.5, and 3.0. The vertical flight times are varied from 1
second to 24 seconds, and the maximum programmed tilt angle is varied
from 2 to 90 degrees. The trajectory calculations are continued in all
cases for a total time, $T = 0.9T_u$, i.e., a mass ratio of 10.

Approximately one hundred trajectories were computed for this
paper. Table IV lists values of mass ratio, velocity, altitude, flight
path angle, energy, scalar velocity loss due to drag, and scalar velocity
loss due to gravity for some of the more useful trajectories. The effects
of varying the parameters, n_i, T_v, and U_m, are shown in Figs. 5 through 18,
which display burnout values of velocity, altitude, energy, and flight
path angle plotted against maximum programmed tilt angle for a mass ratio
of 10. Separate plots are shown for each vertical flight time used.

Scalar velocity loss due to drag is shown in Figs.19 through 22.
V_D, divided by the ballistic coefficient, $W_i/C_{D_o}A$, is plotted versus burnout
flight path angle for each n_i and each T_v. A more general presentation is
obtained with the ballistic coefficient, which uses the value of C_{D_o} at Mach
2.0.

Since side loading is an important consideration in large rocket design, plots of the maximum lift load factor versus U_m for each n_i and each T_v are included as Figs. 23 through 26.

The length of time that the rocket is subjected to lift loads is also of interest. Figure 27 shows the time required to tilt the missile so that it will attain a burnout flight path angle of thirty degrees. This is plotted against n_i to show the large increase in time required for tilting as n_i is increased.

An optimization study is made, based on finding the combination of parameters which would give the highest specific energy at burnout for each n_i investigated. Energy is first maximized for fixed values of γ_b by plotting energy versus the value of U_m corresponding to particular vertical flight times. The maximum energy points are then cross-plotted against γ_b and the value of U_m corresponding to the maximum energy point for the fixed values of γ_b. As a cross-check, this procedure is reversed so that energy is maximized for fixed values of U_m, and cross-plotted in the same manner. Also included in these figures are the values of burnout velocity and burnout altitude which occur at the maximum energy points. The optimization results are shown in Figs. 29 through 31.

Representative trajectories for various values of n_i are identified in detail in Table V. These particular trajectories were chosen because they were closest to the maximum energy trajectories for each case.

TABLE IV

TRAJECTORIES INVESTIGATED SHOWING BURNOUT

VALUES FOR VARIOUS VALUES OF MASS RATIO

$$n_i = 1.5$$

T_v	U_m	T_b	MR	V_b	Y_b	γ_b	$E_b \times 10^{-8}$	V_D	V_G
8	2	13*	1.07	232	1,463	87.8	.001	.59	420
		141	3.39	7,190	285,739	53.5	.350	422	4,188
		161	5.13	10,684	423,565	50.9	.707	422	4,694
		180	10.0	16,700	616,000	49.0	1.590	422	5,078
8	6	14*	1.08	252	1,703	83.6	.001	.78	483
		142	3.45	8,169	165,530	14.8	.387	749	3,032
		162	5.26	12,086	207,113	11.1	.797	779	3,155
		180	10.0	18,130	250,500	8.9	1.670	798	3,272
8	12	17*	1.09	314	2,532	78.2	.001	1.6	516
		141	3.39	4,843	363,871	-11.3	.129	5,083	1,874
		161	5.13	2,970	140,962	-20.3	.048	11,142	1,688
16	4	26*	1.15	506	6,214	86.0	.003	5.91	838
		142	3.45	7,204	305,300	61.4	.358	407	4,339
		162	5.26	10,731	458,176	59.6	.723	407	4,882
		180	10.0	16,400	650,700	58.0	1.553	407	5,393
16	8	27*	1.16	529	6,715	82.0	.004	6.80	894
		139	3.28	7,136	248,475	41.8	.334	465	3,899
		159	4.88	10,565	358,888	38.4	.674	465	4,220
		180	10.0	17,100	525,000	36.0	1.628	465	4,635
16	12	29*	1.17	577	7,782	78.0	.004	8.79	949
		141	3.39	7,754	212,551	27.0	.369	556	3,490
		161	5.13	11,484	290,231	23.3	.753	559	3,757
		180	10.0	17,700	388,000	21.0	1.680	559	3,941
16	18	31*	1.18	627	8,900	72.8	.005	11.3	952
		139	3.28	7,727	147,717	12.9	.346	821	2,952
		159	4.88	11,392	180,348	9.0	.706	878	2,980
		180	10.0	18,181	216,304	5.8	1.722	937	3,082

* Completion of tilt phase. ($\alpha = 0$).

TABLE IV (Continued)

$$n_i = 1.5$$

T_v	U_m	T_b	MR	V_b	Y_b	γ_b	$E_b \times 10^{-8}$	V_D	V_G
24	6	39*	1.24	824	14,793	83.6	.008	21.5	1,230
		139	3.28	6,755	291,072	66.0	.321	404	4,341
		159	4.88	10,014	439,719	63.6	.643	404	4,832
		180	10.0	16,300	676,000	62.3	1.546	404	5,496
24	12	41*	1.26	878	16,392	78.0	.009	26.5	1,326
		141	3.39	7,310	270,316	46.5	.354	443	3,747
		161	5.13	10,859	395,063	43.5	.717	443	4,498
		180	10.0	16,830	566,000	41.5	1.597	443	4,927
24	24	45*	1.29	988	19,658	66.0	.011	42.9	1,429
		141	3.39	7,849	190,631	21.7	.369	626	3,025
		161	5.13	11,630	252,472	17.8	.757	634	3,536
		180	10.0	17,850	326,500	15.5	1.695	636	3,714
24	32	49*	1.33	1,107	23,086	58.0	.014	66.9	1,576
		141	3.39	7,996	141,693	10.8	.365	891	2,613
		161	5.13	11,815	168,429	6.9	.752	979	3,006
		180	10.0	18,095	192,484	4.1	1.699	1,092	3,013

* Completion of tilt phase ($\alpha = 0$)

TABLE IV (Continued)

$$n_i = 2.0$$

T_v	U_m	T_b	MR	V_b	Y_b	γ_b	$E_b \times 10^{-8}$	V_D	V_G
1	4	4*	1.03	133	263	86.0	.0002	.05	152
		104	3.26	7,785	235,616	51.2	.379	658	2,957
		120	5.0	11,520	351,320	49.1	.777	659	3,341
		135	10.0	17,853	510,742	47.5	1.758	659	3,688
1	10	7*	1.05	238	811	80.2	.0005	.34	235
		103	3.08	7,861	175,494	30.4	.365	892	2,047
		119	4.83	11,626	247,918	27.6	.756	902	2,652
		135	10.0	18,406	350,294	25.3	1.807	903	2,891
1	20	12*	1.09	427	2,392	69.1	.002	2.0	401
		104	3.26	7,979	125,765	16.0	.359	1,419	2,002
		120	5.0	11,871	162,216	12.9	.757	1,532	2,117
		135	10.0	18,300	200,000	11.0	1.748	1,623	2,277
1	24	14*	1.10	507	3,250	66.9	.002	3.4	410
		106	3.40	8,216	114,092	12.0	.374	1,720	1,844
		118	4.68	11,042	133,796	9.6	.653	1,901	1,937
		135	10.0	17,980	165,825	6.9	1.669	2,203	2,017
8	10	20*	1.15	732	6,989	80.0	.007	16.5	602
		104	3.26	7,670	251,704	60.1	.375	616	3,114
		120	5.0	11,357	380,350	58.9	.767	616	3,547
		135	10.0	17,620	559,000	58.0	1.729	616	3,964
8	20	25*	1.20	945	10,914	69.8	.008	22.3	793
		105	3.33	8,085	217,596	41.5	.397	738	2,797
		121	5.16	11,998	318,203	39.1	.822	739	3,113
		135	10.0	18,040	443,500	38.6	1.762	739	3,421
8	30	30*	1.25	1,164	15,467	59.8	.012	54.2	937
		106	3.40	8,422	179,763	28.1	.413	938	2,420
		118	4.68	11,317	231,661	26.0	.715	948	2,615
		135	10.0	18,350	332,000	23.9	1.786	950	2,900
8	50	40*	1.36	1,600	25,169	40.9	.021	223	1,142
		104	3.26	7,666	101,365	10.3	.326	1,832	1,902
		120	5.0	11,280	121,199	7.0	.675	2,275	1,965
		135	10.0	17,353	140,363	4.5	1.551	2,848	1,999

* Completion of tilt phase. ($\alpha = 0$)

TABLE IV (Continued)

$n_i = 2.0$

T_v	U_m	T_b	MR	V_b	Y_b	γ_b	$E_b \times 10^{-8}$	V_D	V_G
16	16	37*	1.31	1,422	24,960	74.1	.018	132	1,051
		105	3.33	7,849	255,783	59.4	.390	625	3,146
		121	5.16	11,655	386,045	57.8	.803	625	3,570
		135	10.0	17,715	557,000	56.5	1.700	625	3,860
16	36	46*	1.44	1,782	36,270	54.1	.028	328	2,405
		106	3.40	8,327	196,704	33.3	.410	833	2,620
		118	4.68	11,195	257,436	31.4	.710	837	2,848
		135	10.0	18,180	376,000	29.0	1.795	838	3,182
16	48	51*	1.52	2,030	41,966	42.6	.034	447	1,583
		103	3.08	7,807	147,843	22.7	.352	1,031	1,962
		119	4.83	11,609	200,871	19.7	.739	1,068	2,503
		135	10.0	18,444	273,141	17.3	1.790	1,081	2,675
16	60	58*	1.63	2,463	42,291	30.1	.046	604	1,663
		106	3.40	8,253	118,317	12.4	.379	1,436	2,091
		118	4.68	11,107	139,002	10.0	.661	1,587	2,186
		135	10.0	18,102	173,138	7.4	1.690	1,828	2,270
24	12	49*	1.48	1,905	44,785	78.1	.033	347	1,533
		105	3.33	7,745	271,198	71.2	.387	590	3,285
		121	5.16	11,504	413,804	70.1	.795	590	3,756
		135	10.0	17,420	597,000	69.3	1.759	590	4,190
24	30	56*	1.59	2,281	56,032	60.0	.044	468	1,726
		104	3.26	7,757	226,562	48.2	.374	670	2,973
		120	5.0	11,511	336,484	46.0	.771	671	3,338
		135	10.0	17,863	487,562	44.3	1.750	671	3,666
24	50	65*	1.76	2,905	68,846	40.2	.064	626	1,929
		105	3.33	8,136	176,979	28.4	.388	842	2,642
		121	5.16	12,140	247,294	25.6	.816	853	2,857
		135	10.0	18,317	332,589	23.6	1.780	854	3,029
24	70	77*	2.05	4,012	80,808	20.0	.106	845	2,073
		105	3.33	8,105	121,804	12.1	.367	1,190	2,325
		121	5.16	12,099	148,534	9.1	.780	1,350	2,401
		135	10.0	18,222	175,684	6.9	1.717	1,531	2,447

* Completion of tilt phase. ($\alpha = 0$)

TABLE IV (Continued)

$$n_i = 2.5$$

T_v	U_m	T_b	MR	V_b	Y_b	γ_b	$E_b \times 10^{-8}$	V_D	V_G
1	10	8*	1.07	410	3,634	79.7	.003	3.5	242
		84	3.33	8,343	223,832	59.8	.420	794	2,483
		96	5.0	11,927	326,512	58.6	.816	795	2,798
		108	10.0	18,292	476,217	57.6	1.826	795	3,113
1	20	15*	1.14	810	5,638	69.9	.005	9.32	445
		83	3.24	8,200	189,882	45.9	.397	926	2,224
		95	4.78	11,711	272,461	44.2	.773	931	2,418
		108	10.0	18,511	402,888	42.7	1.843	931	2,758
1	40	27*	1.29	1,527	17,249	50.4	.017	138	795
		83	3.24	8,125	136,994	27.3	.374	1399	1,826
		95	4.78	11,696	187,321	25.1	.744	1447	1,917
		108	10.0	18,595	264,277	23.2	1.814	1465	2,140
1	60	39*	1.48	2,218	30,093	30.5	.034	546	1,016
		83	3.24	7,450	86,735	12.4	.305	2419	1,474
		95	4.78	10,547	105,551	9.8	.590	3038	1,485
		108	10.0	16,722	129,978	7.5	1.440	3888	1,590
8	20	29*	1.32	1,584	21,891	70.0	.020	167	929
		85	3.42	8,556	225,510	57.7	.438	834	2,490
		97	5.18	12,286	328,567	56.5	.860	835	2,779
		108	10.0	18,200	465,000	56.0	1.670	835	3,165
8	30	34*	1.40	1,846	28,971	60.2	.026	310	1,084
		82	3.16	7,898	182,871	46.5	.371	941	2,261
		94	4.58	11,284	263,301	44.8	.721	947	2,449
		108	10.0	18,437	402,241	43.2	1.829	947	2,816
8	50	44*	1.58	2,497	42,862	40.5	.045	623	1,300
		84	3.33	8,367	143,370	27.6	.396	1284	1,969
		96	5.0	12,074	195,898	25.5	.792	1324	2,122
		108	10.0	18,593	269,376	23.7	1.815	1338	2,269
8	60	50*	1.72	3,012	50,266	30.1	.062	804	1,414
		82	3.16	7,750	112,553	19.8	.336	1554	1,806
		94	4.58	11,150	146,717	17.5	.669	1700	1,830
		108	10.0	18,300	201,300	16.0	1.740	1823	2,077

* Completion of tilt phase. ($\alpha = 0$)

TABLE IV (Continued)

$n_i = 2.5$

T_v	U_m	T_b	MR	V_b	Y_b	γ_b	$E_b \times 10^{-8}$	V_D	V_G
16	20	43*	1.56	2,405	48,461	70.1	.044	510	1,365
		83	3.24	8,038	220,466	64.0	.394	780	2,532
		95	4.78	11,479	323,466	62.8	.763	781	2,800
		108	10.0	18,300	489,000	62.0	1.814	781	3,119
16	48	56*	1.88	3,593	72,694	42.3	0.088	801	1,706
		84	3.33	8,385	169,554	35.6	.406	1011	2,224
		96	5.0	12,071	237,219	33.6	.805	1024	2,425
		108	10.0	18,553	333,571	32.4	1.828	1026	2,621
16	60	67*	2.26	5,030	92,937	30.0	0.156	1017	1,823
		83	3.24	8,123	139,010	25.7	.375	1163	2,064
		95	4.78	11,706	186,315	23.5	.745	1209	2,145
		108	10.0	18,614	258,262	21.5	1.816	1228	2,458
16	70	70*	2.40	5,467	91,502	20.2	.179	1140	1,843
		82	3.16	7,812	116,156	17.8	.342	1323	1,975
		94	4.58	11,240	146,665	15.4	.679	1454	1,986
		108	10.0	18,474	194,613	13.2	1.769	1576	2,150
24	10	55*	1.85	3,530	84,985	80.0	.090	629	1,781
		83	3.24	8,015	236,080	78.4	.397	703	2,632
		95	4.78	11,423	348,703	77.9	.765	703	2,934
		108	10.0	18,101	530,669	77.5	1.809	703	3,396
24	20	59*	1.97	3,974	96,975	70.0	.110	680	1,896
		83	3.24	8,034	226,042	67.5	.395	732	2,584
		95	4.78	11,464	332,126	66.6	.764	733	2,863
		108	10.0	18,120	502,000	65.5	1.811	733	3,347
24	40	68*	2.3	5,174	121,421	49.8	.173	816	2,060
		84	3.33	8,312	200,512	47.7	.410	844	2,464
		96	5.0	11,946	287,122	46.1	.806	847	2,927
		108	10.0	18,364	412,507	45.0	1.819	847	2,987
24	60	83*	3.24	8,054	160,548	30.0	.376	983	2,323
		95	4.78	11,636	216,654	28.5	.747	1001	2,423
		108	10.0	18,525	303,506	26.6	1.813	1005	2,670

* Completion of tilt phase. ($\alpha = 0$)

TABLE IV (Continued)

$$n_i = 3.0$$

T_v	U_m	T_b	MR	V_b	Y_b	γ_b	E_bx10^{-8}	V_D	V_G
1	16	14*	1.16	999	6,606	74.2	0.007	14.1	417
		70	3.33	8,603	197,650	61.5	0.434	942	2,078
		78	4.53	11,370	266,817	60.7	0.732	944	2,306
		90	10.0	18,648	417,702	60.0	1.873	945	2,607
1	24	20*	1.25	1,448	13,350	66.1	0.015	84.8	622
		68	3.12	8,031	168,876	53.0	0.377	1,051	1,898
		80	5.0	12,257	262,685	51.5	0.836	1,061	2,202
		90	10.0	18,700	378,000	50.5	1.867	1,061	2,439
1	40	30*	1.43	2,141	27,467	50.1	0.032	418	901
		70	3.33	8,519	148,091	37.9	0.410	1,360	1,741
		78	4.55	11,335	195,038	36.6	0.705	1,384	1,901
		90	10.0	18,714	296,016	35.0	1.846	1,393	2,093
1	52	37*	1.59	2,716	376,444	38.1	0.049	714	1,050
		69	3.23	8,072	118,215	28.2	0.364	1,665	1,583
		81	5.26	12,515	171,985	26.1	0.838	1,776	1,739
		90	10.0	18,500	230,000	25.0	1.770	1,818	1,882
8	10	27*	1.37	1,895	25,477	80.1	0.026	279	866
		71	3.44	8,816	219,839	76.0	0.459	895	2,209
		79	4.76	11,682	298,606	75.6	0.778	896	2,472
		90	10.0	18,503	454,492	75.1	1.858	896	2,801
8	20	32*	1.47	2,257	34,766	70.1	0.037	451	1,012
		68	3.13	7,975	184,230	64.2	0.377	954	2,051
		80	5.0	12,163	290,286	63.2	0.833	958	2,399
		90	10.0	18,570	423,328	62.4	1.860	959	2,671
8	40	42*	1.73	3,212	54,483	50.1	0.069	722	1,366
		70	3.33	8,559	163,808	44.0	0.419	1,144	1,917
		78	4.55	11,366	217,461	42.7	0.716	1,156	2,098
		90	10.0	18,718	333,471	41.5	1.859	1,160	2,322
8	60	53*	2.13	4,681	73,877	30.2	0.133	1,148	1,471
		69	3.23	8,135	120,154	26.8	0.369	1,473	1,712
		81	5.26	12,599	171,518	24.6	0.849	1,572	1,859
		90	10.0	18,644	226,562	23.2	1.811	1,607	1,949

* Completion of tilt phase. ($\alpha = 0$)

TABLE IV (Continued)

$$n_i = 3.0$$

T_v	U_m	T_b	MR	V_b	Y_b	γ_b	$E_b \times 10^{-8}$	V_D	V_G
16	16	45*	1.82	3,606	71,902	74.1	0.088	728	1,446
		69	3.23	8,264	201,053	72.0	0.406	871	2,235
		81	5.26	12,623	317,617	71.3	0.899	874	2,533
		90	10.0	18,550	451,000	71.0	1.865	874	2,776
16	32	52*	2.08	4,584	92,482	58.2	0.135	878	1,598
		68	3.13	7,986	174,404	56.0	0.375	962	1,532
		80	5.0	12,201	271,637	54.4	0.832	969	2,350
		90	10.0	18,600	394,000	54.0	1.857	970	2,630
16	60	70	3.33	8,487	144,099	30.4	0.406	1,196	1,937
		72*	3.57	9,112	152,911	30.1	0.464	1,204	1,984
		80	5.0	12,209	194,233	29.3	0.808	1,230	2,081
		90	10.0	18,735	265,485	27.8	1.840	1,243	2,222
16	90	70	3.33	8,139	120,218	12.1	0.370	1,431	2,050
		80	5.0	11,824	134,099	6.2	0.742	1,574	2,122
		90	10.0	18,169	143,873	2.7	1.697	1,882	2,149
24	20	67*	3.03	7,747	186,250	70.1	0.360	827	2,126
		71	3.44	8,871	217,397	70.0	0.463	830	2,219
		79	4.76	11,746	293,980	69.4	0.784	831	2,473
		90	10.0	18,550	442,800	69.0	1.863	831	2,819
24	40	70	3.33	8,499	186,774	51.5	0.421	949	2,172
		80*	5.0	12,161	265,425	50.0	0.825	953	2,406
		90	10.0	18,550	379,300	49.5	1.842	954	2,696
24	60	70	3.33	8,317	169,663	37.8	0.400	1,047	2,256
		80	5.0	12,019	227,544	34.0	0.795	1,057	2,444
		90	10.0	18,528	327,434	32.0	1.808	1,059	2,613
24	90	70	3.33	7,968	162,805	29.3	0.370	1,094	2,558
		80	5.0	11,449	198,428	18.1	0.719	1,119	2,952
		90	10.0	17,876	230,643	10.5	1.672	1,135	3,189

* Completion of tilt phase. ($\alpha = 0$)
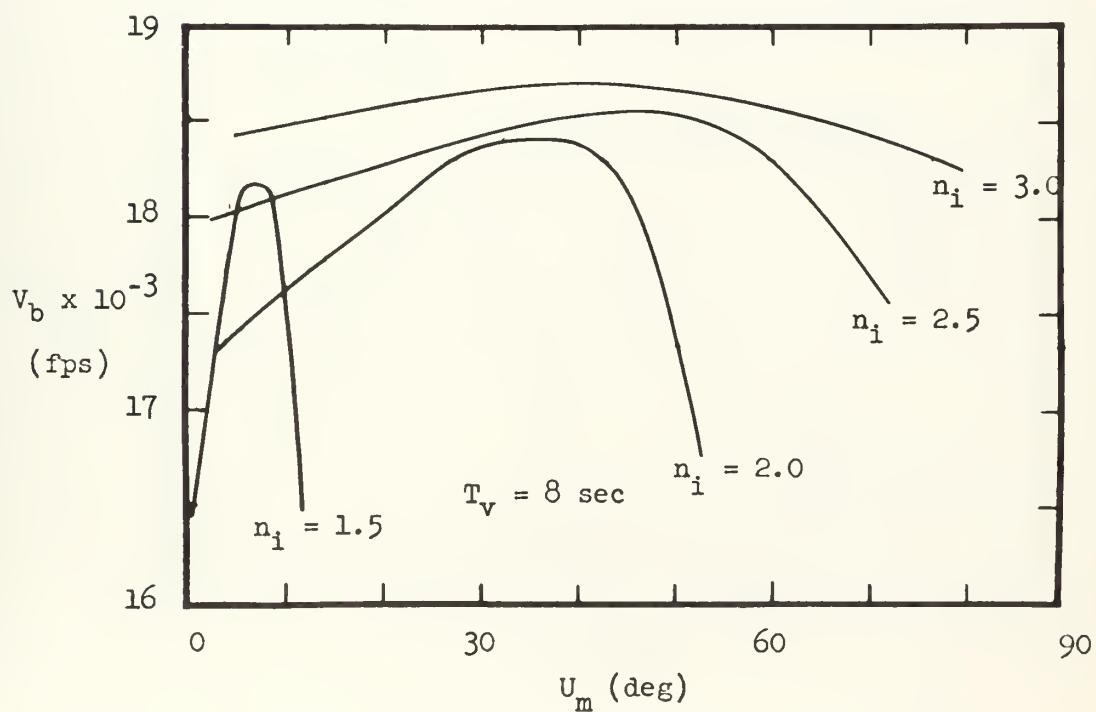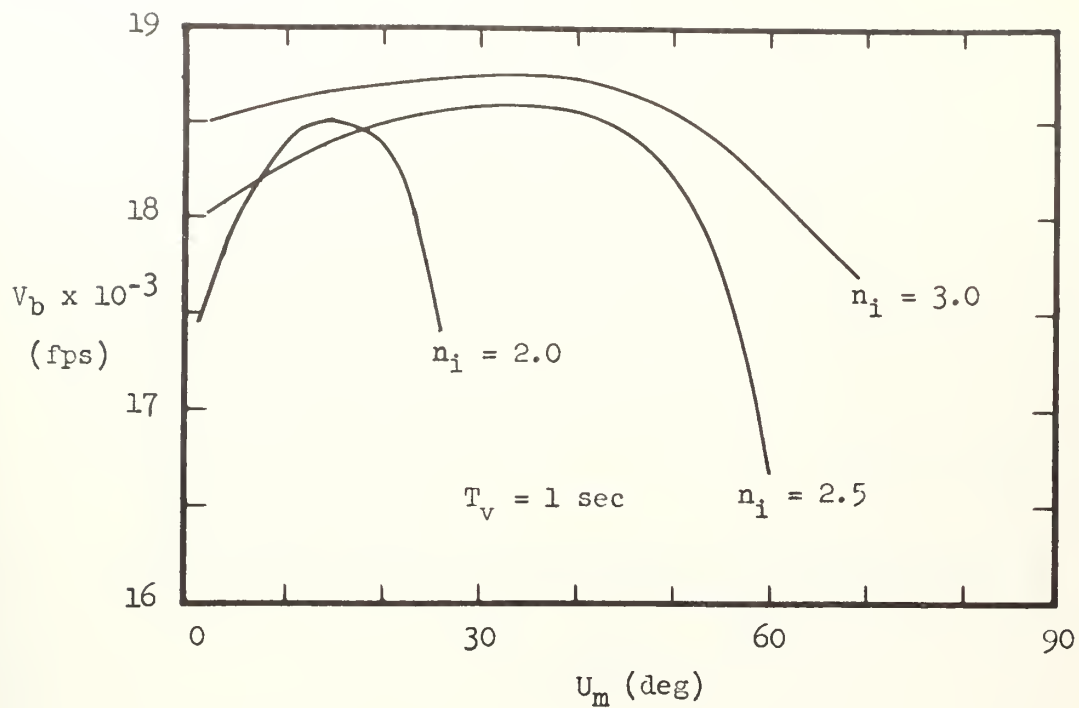
Fig. 5   Variation of V_b with U_m for various values of n_i at a T_v of 1 and 8 seconds.

19

$V_b \times 10^{-3}$
(fps)

18

$n_i = 3.0$

$n_i = 2.5$

17

$n_i = 2.0$

$T_v = 16$ sec

16

$n_i = 1.5$

0   30   60   90

U_m (deg)

19

$n_i = 3.0$

$V_b \times 10^{-3}$
(fps)

18

$n_i = 2.5$

$n_i = 2.0$

17

$T_v = 24$ sec

$n_i = 1.5$

16

0   30   60   90

U_m (deg)
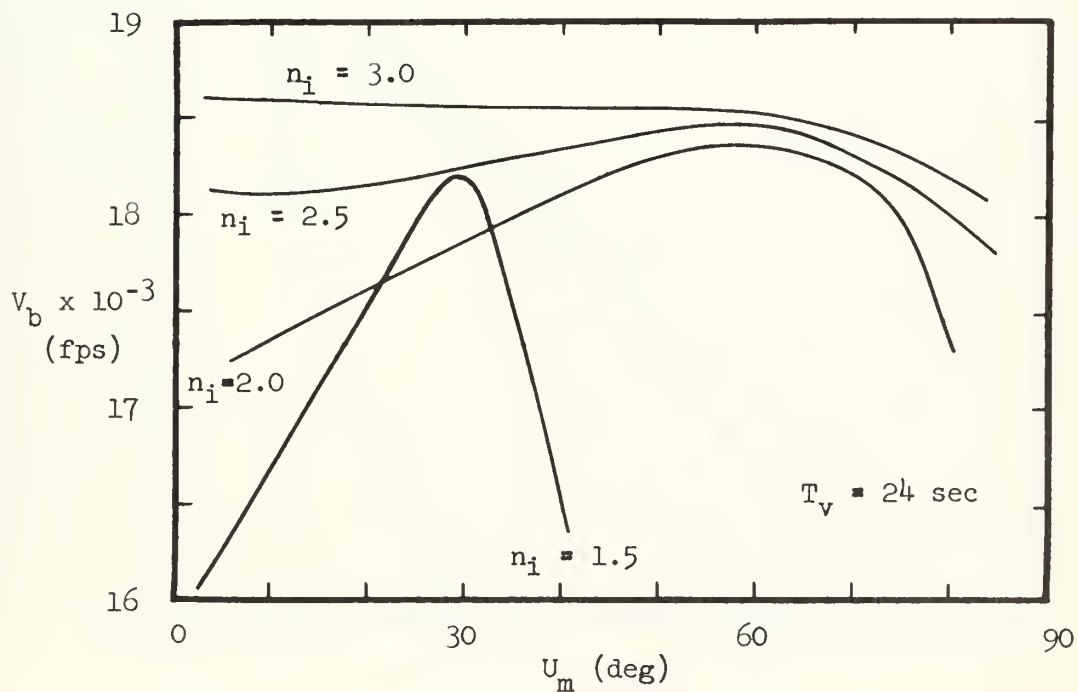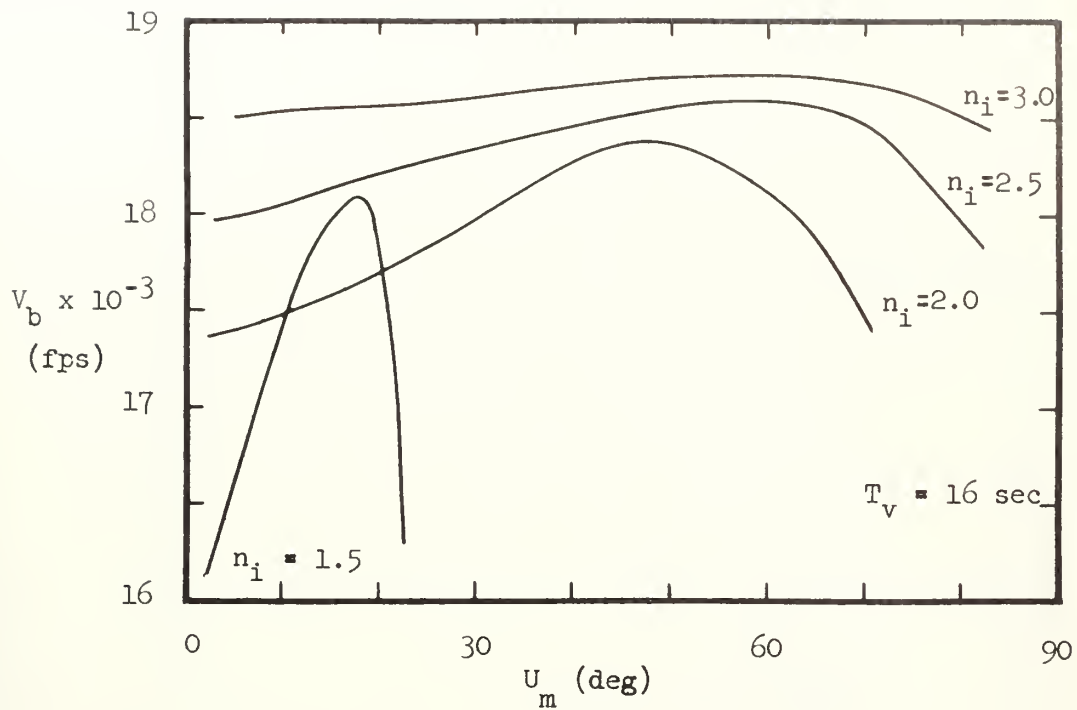
Fig. 6   Variation of V_b with U_m for various values of n_i at a
T_v of 16 and 24 seconds.
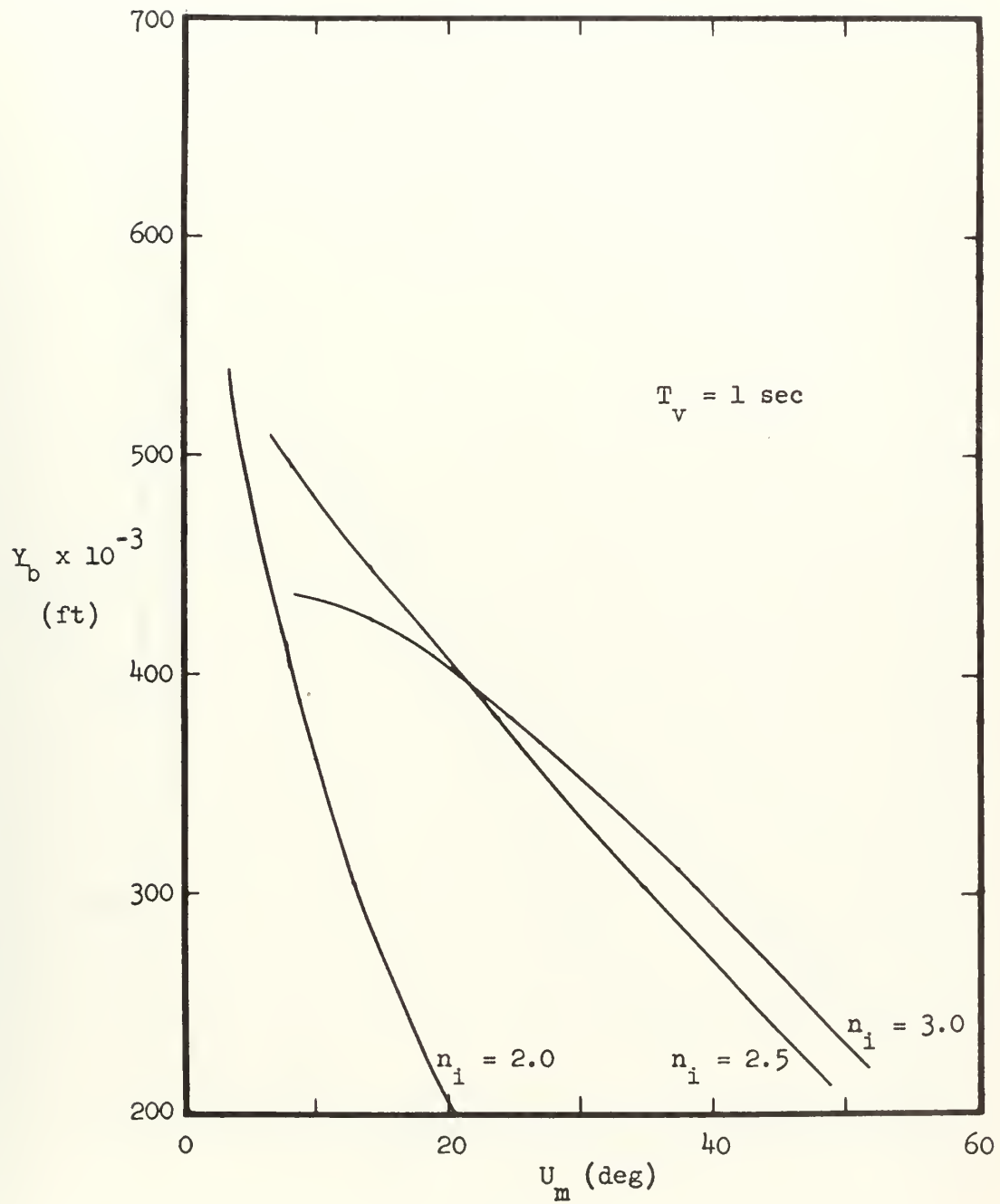
Fig. 7 Variation of Y_b with U_m for various values of n_i at a T_v of 1 second.
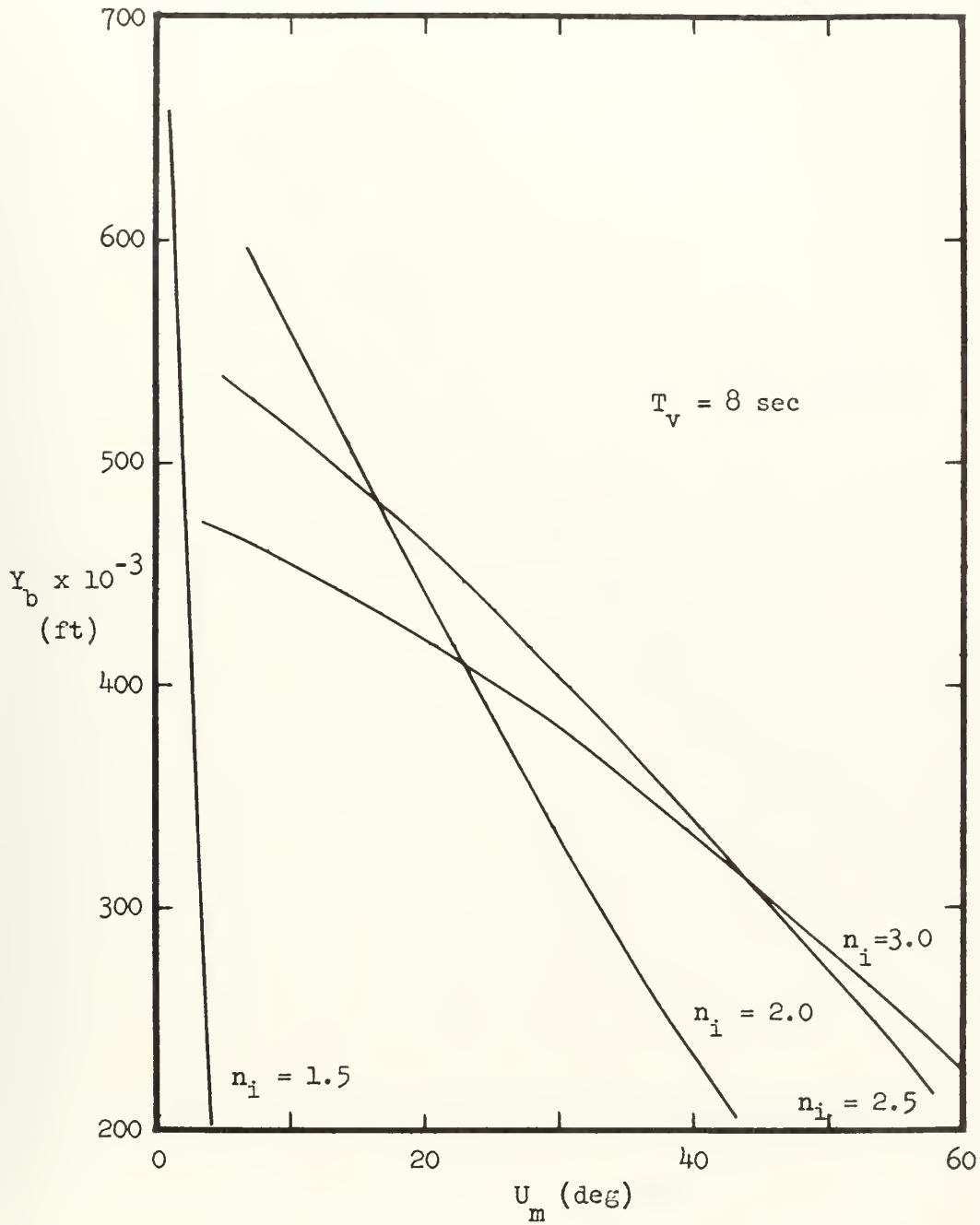
Fig. 8   Variation of Y_b with U_m for various values of n_i at a T_v of 8 seconds.
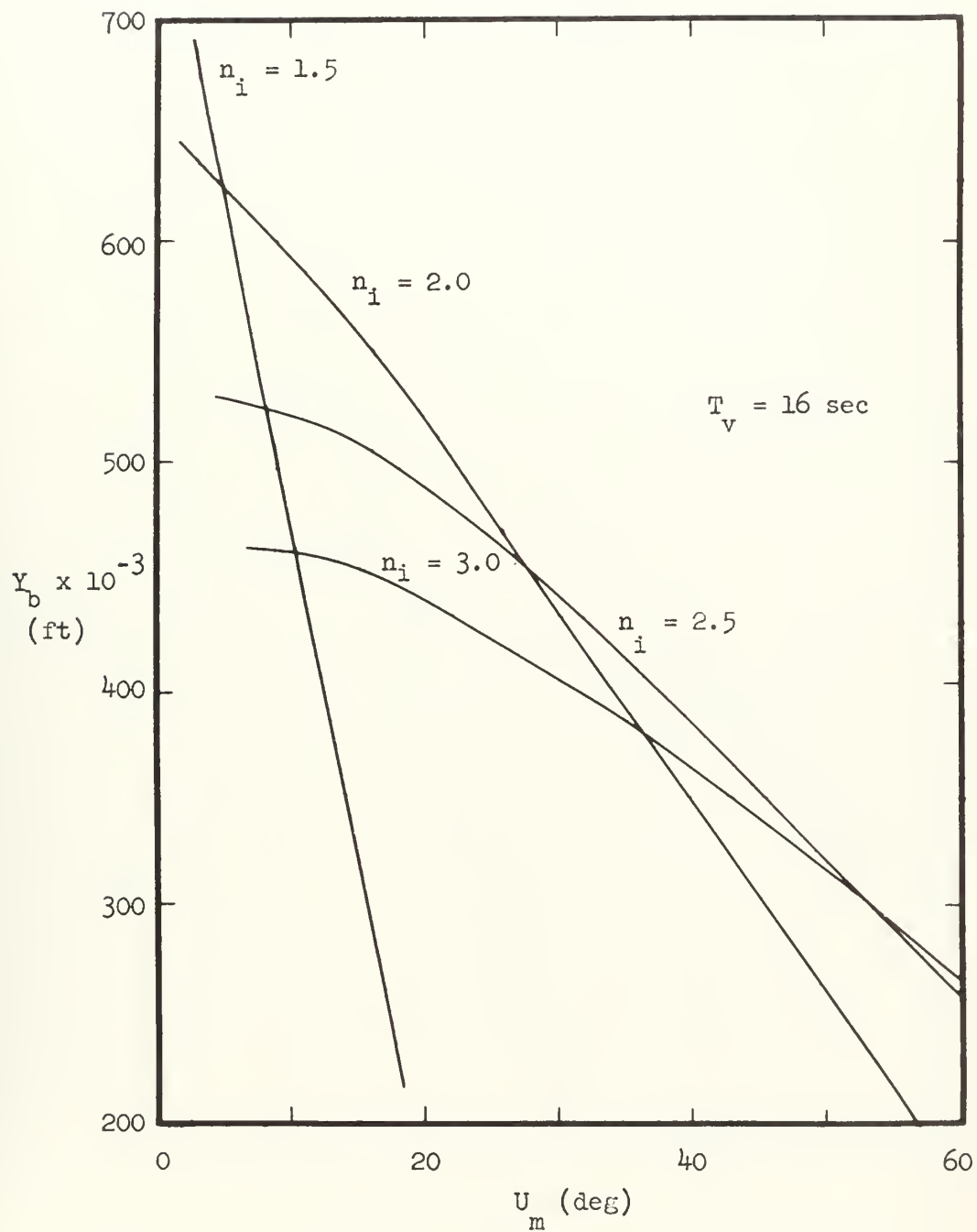
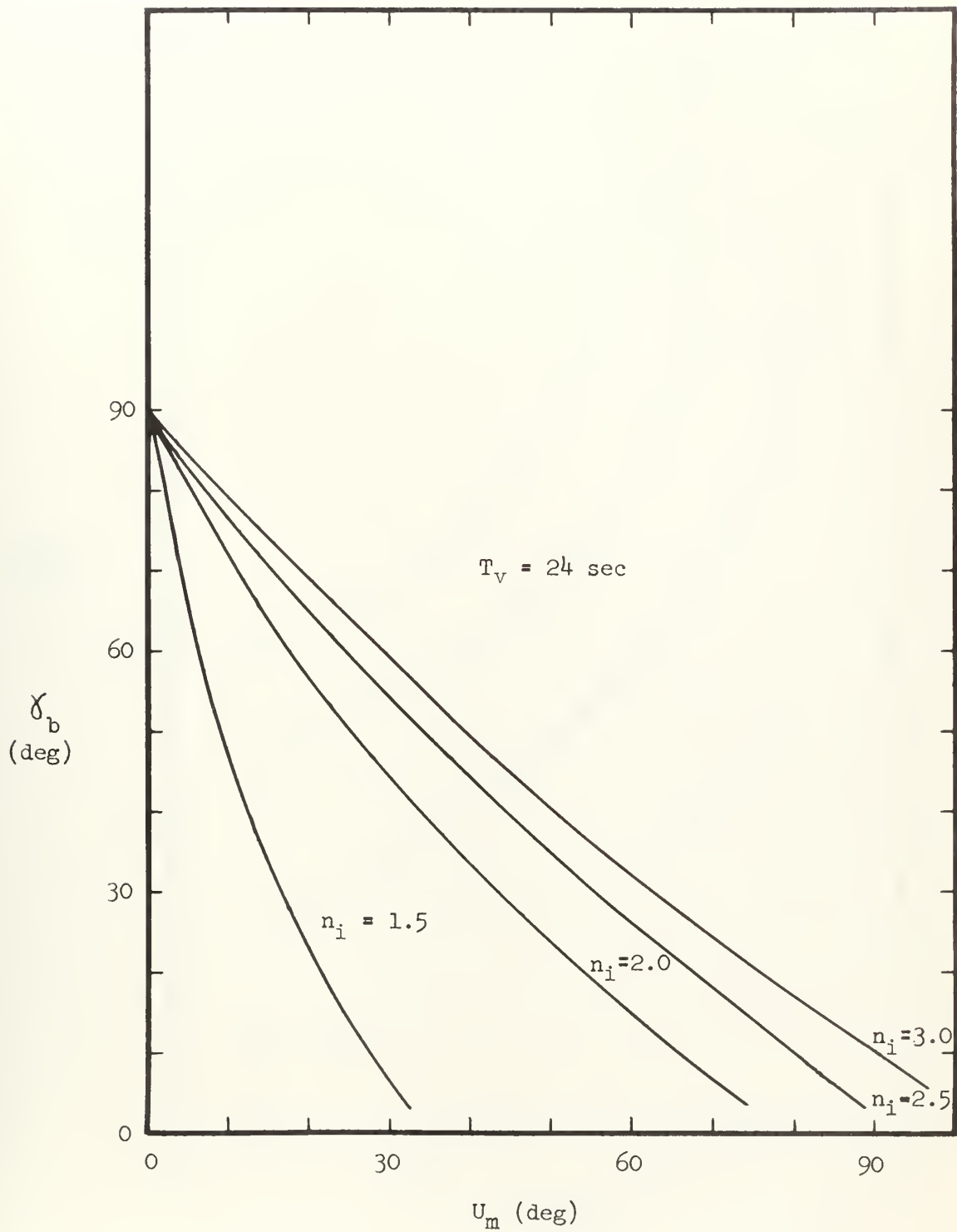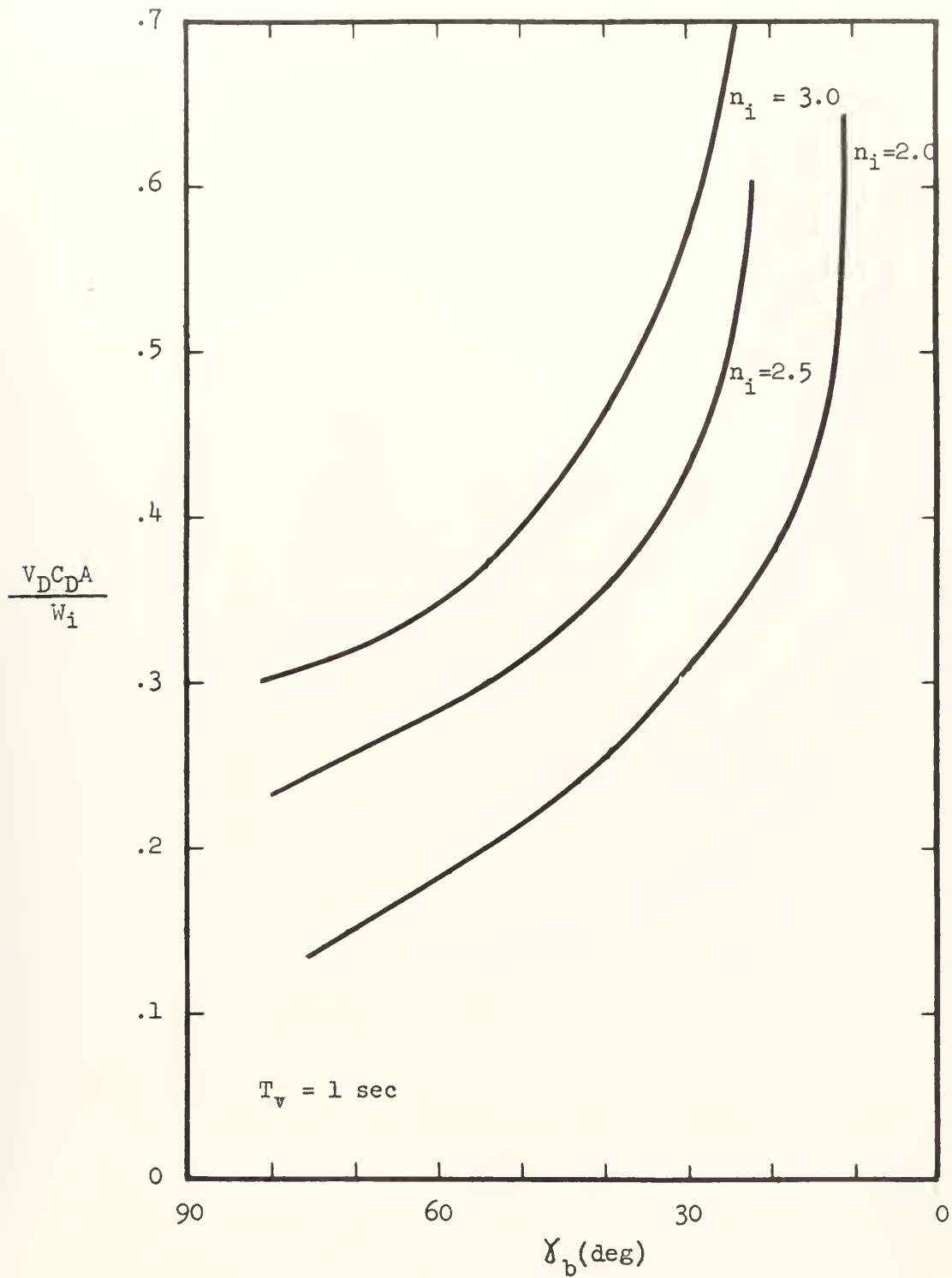Fig. 9   Variation of Y_b with U_m for various values of n_i at a T_v of 16 seconds.
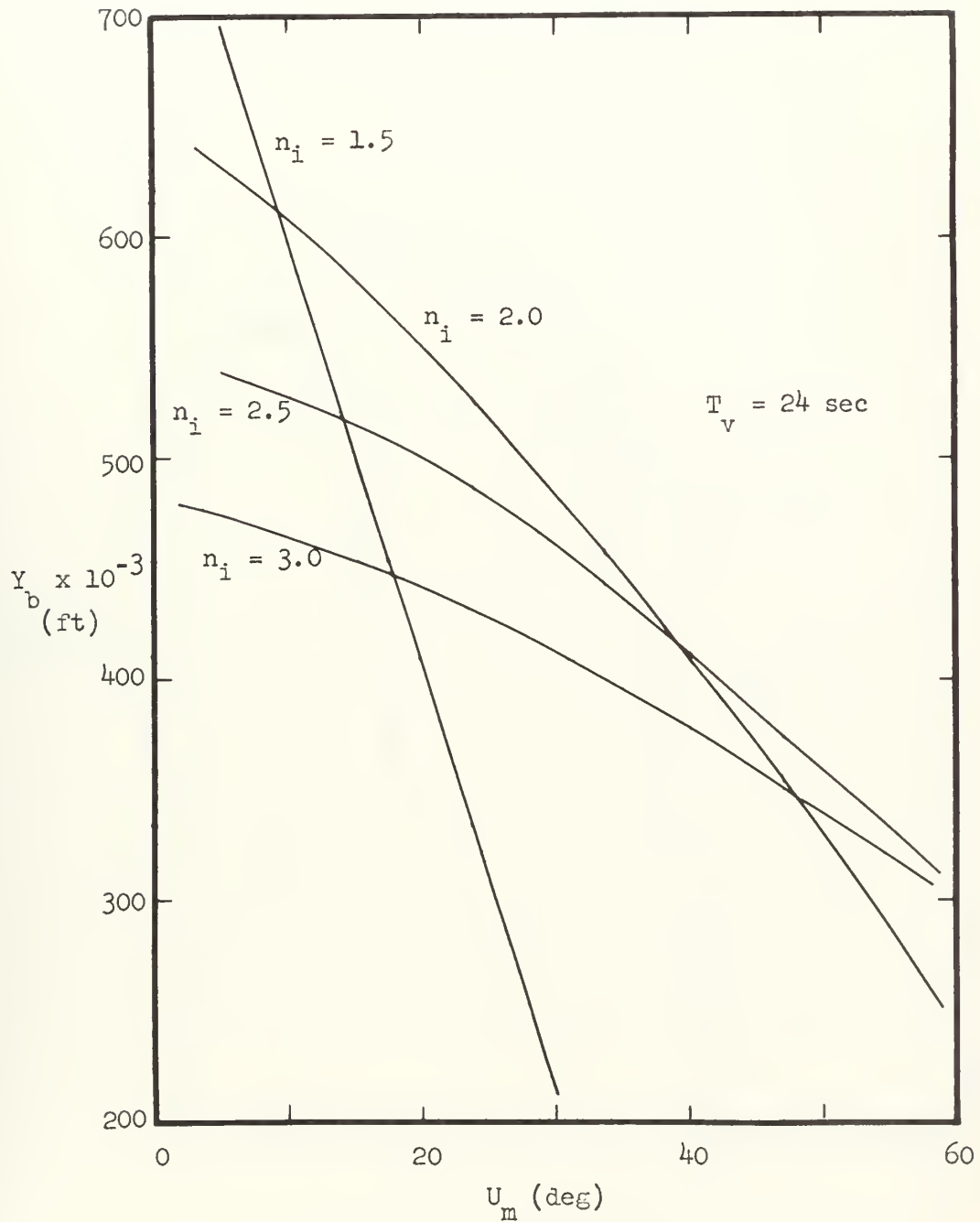
Fig. 10   Variation of Y_b with U_m for various values of n_i at a T_v of 24 seconds.
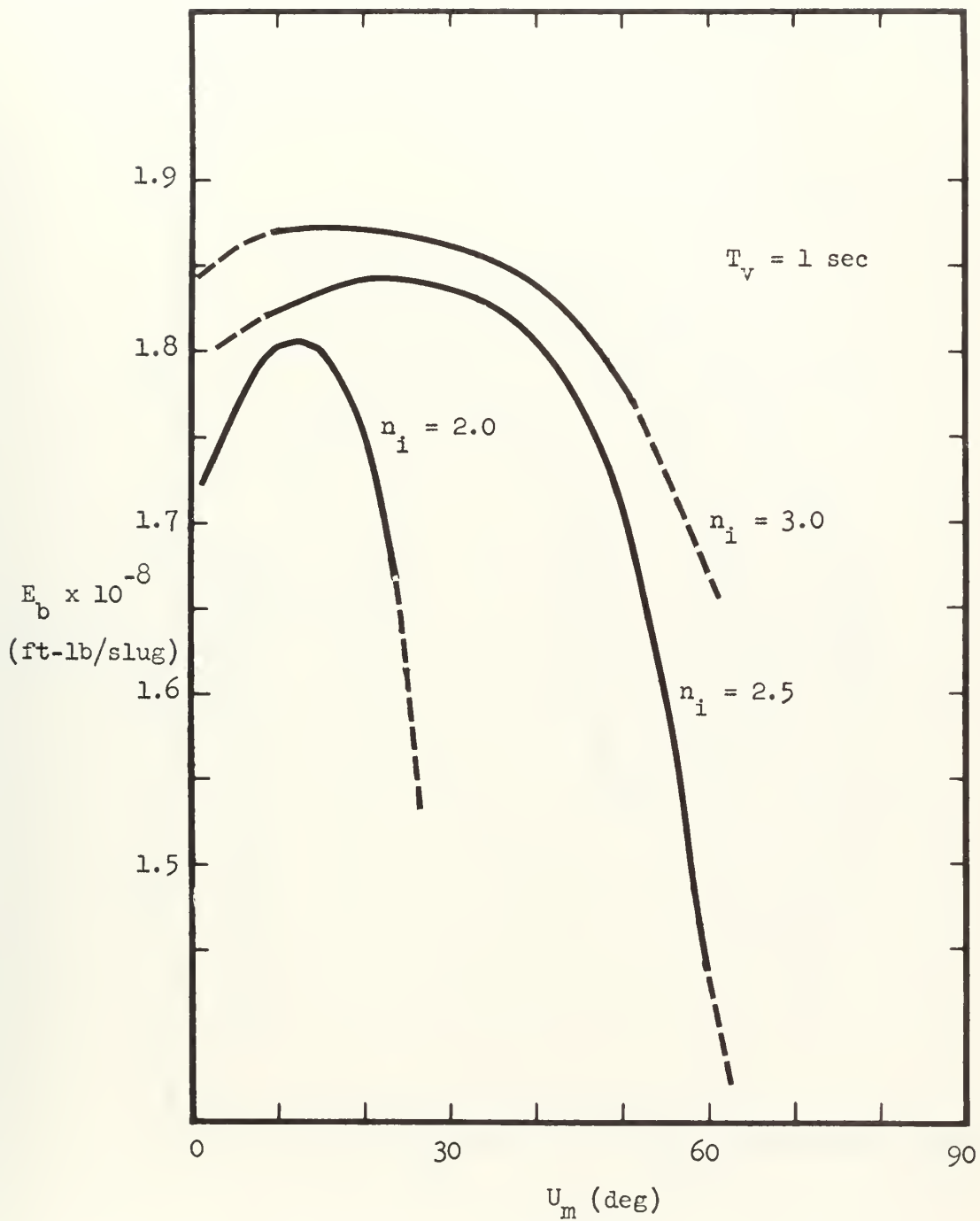
Fig. 11   Variation of E_b with U_m for various values of n_i at a T_v of 1 second.
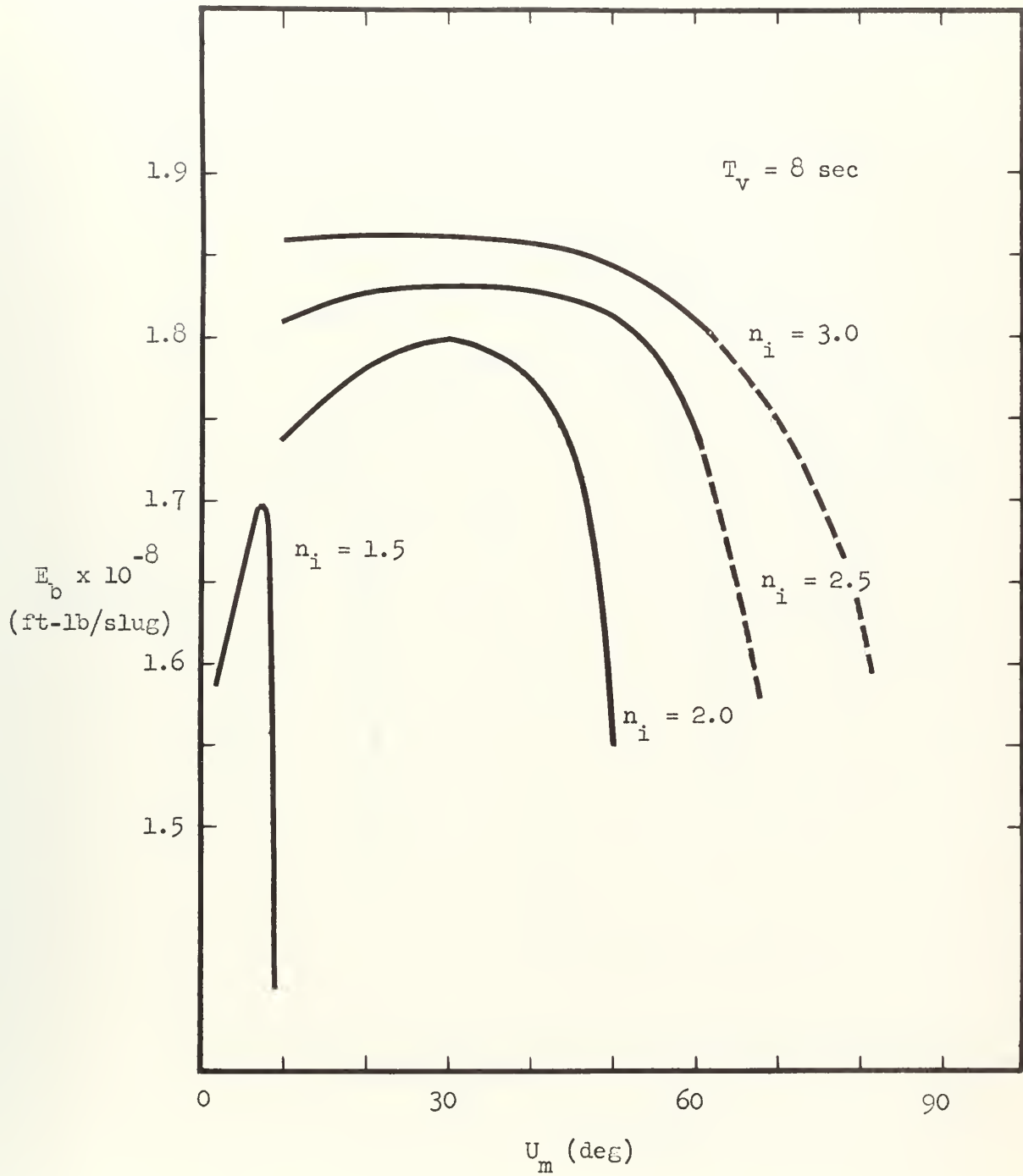
Fig. 12   Variation of E_b with U_m for various values of n_i at a T_v of 8 seconds.
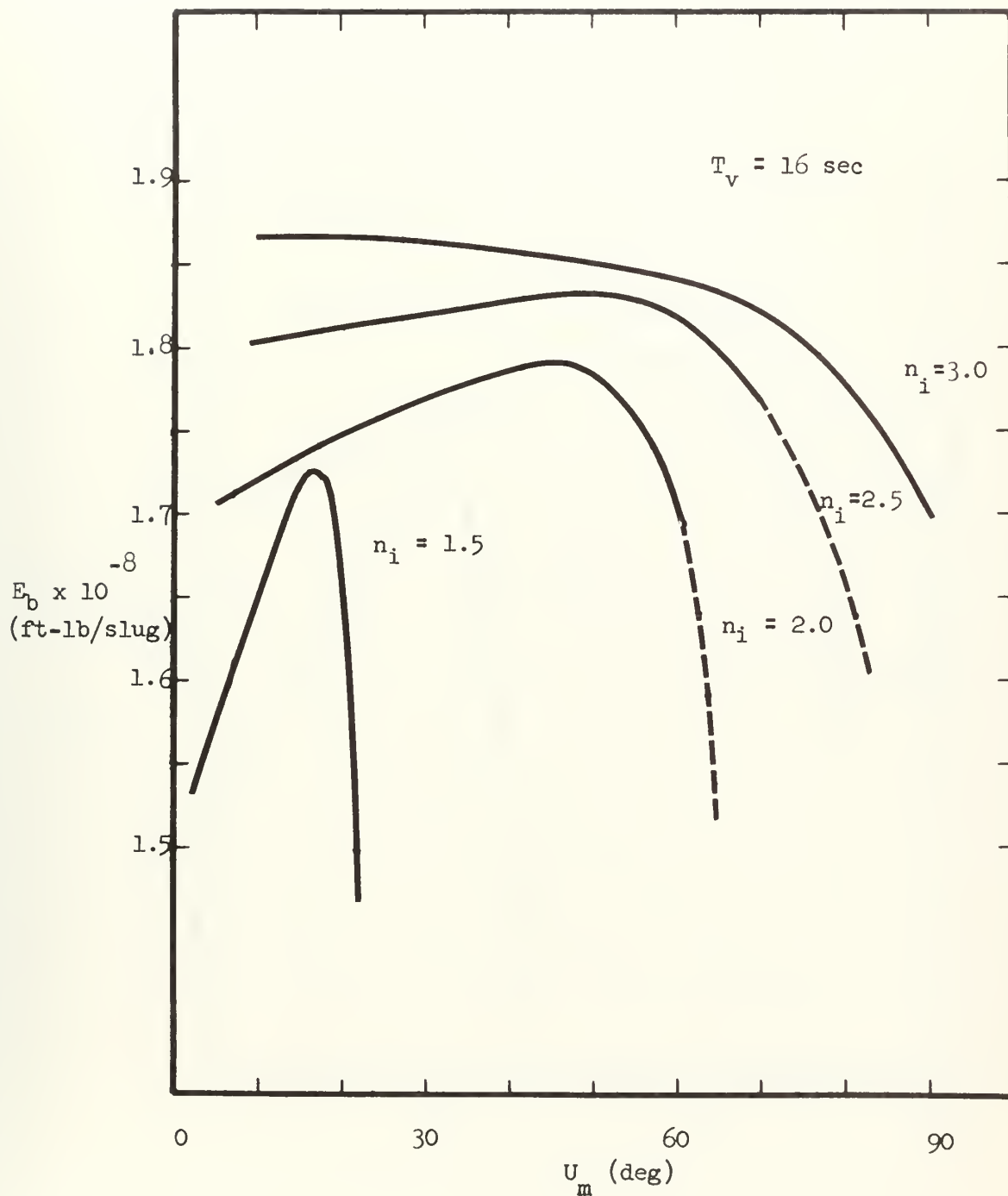
Fig. 13   Variation of E_b with U_m for various values of n_i at a T_v of 16 seconds.
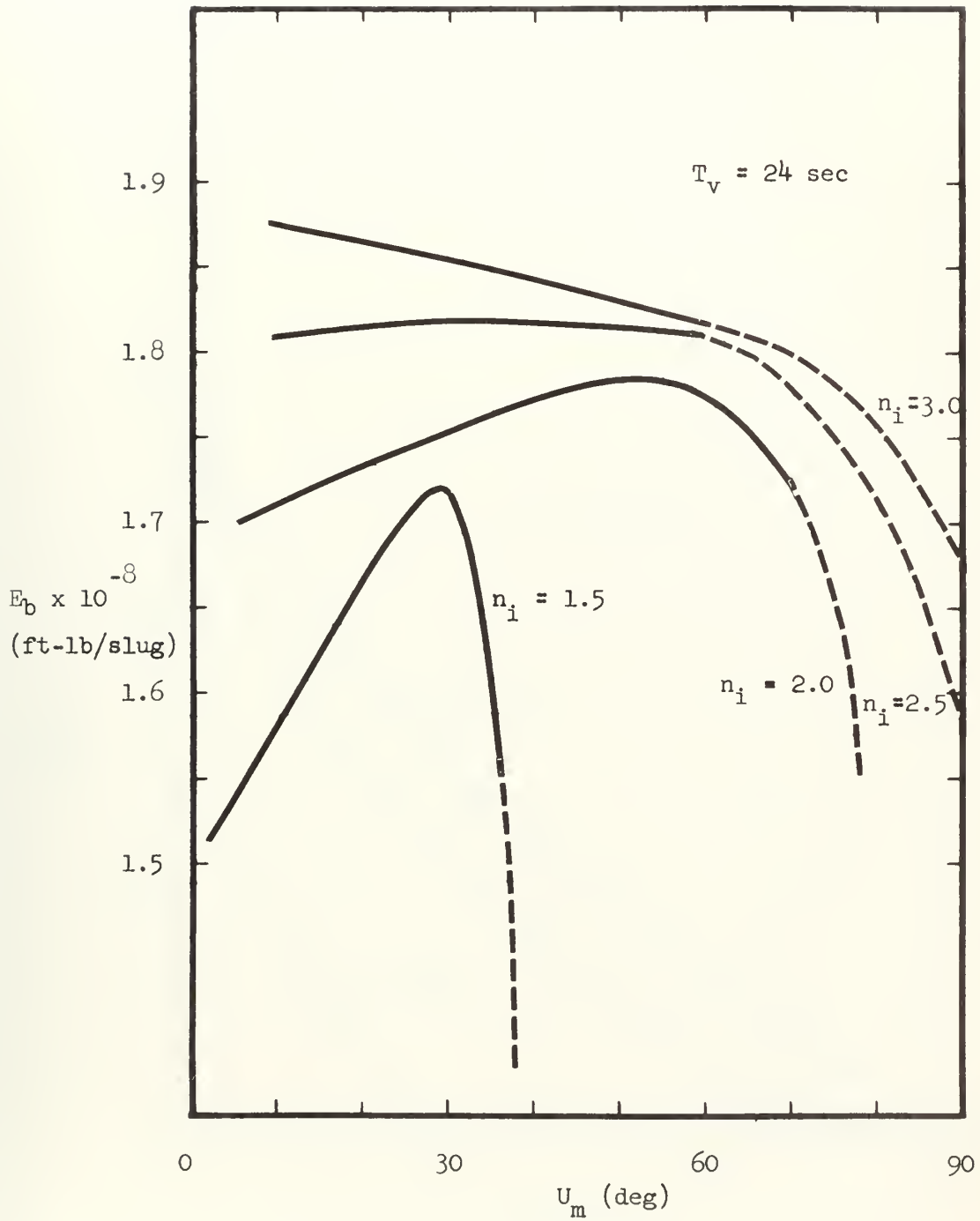
Fig. 14   Variation of E_b with U_m for various values of n_i at a T_v of 24 seconds.
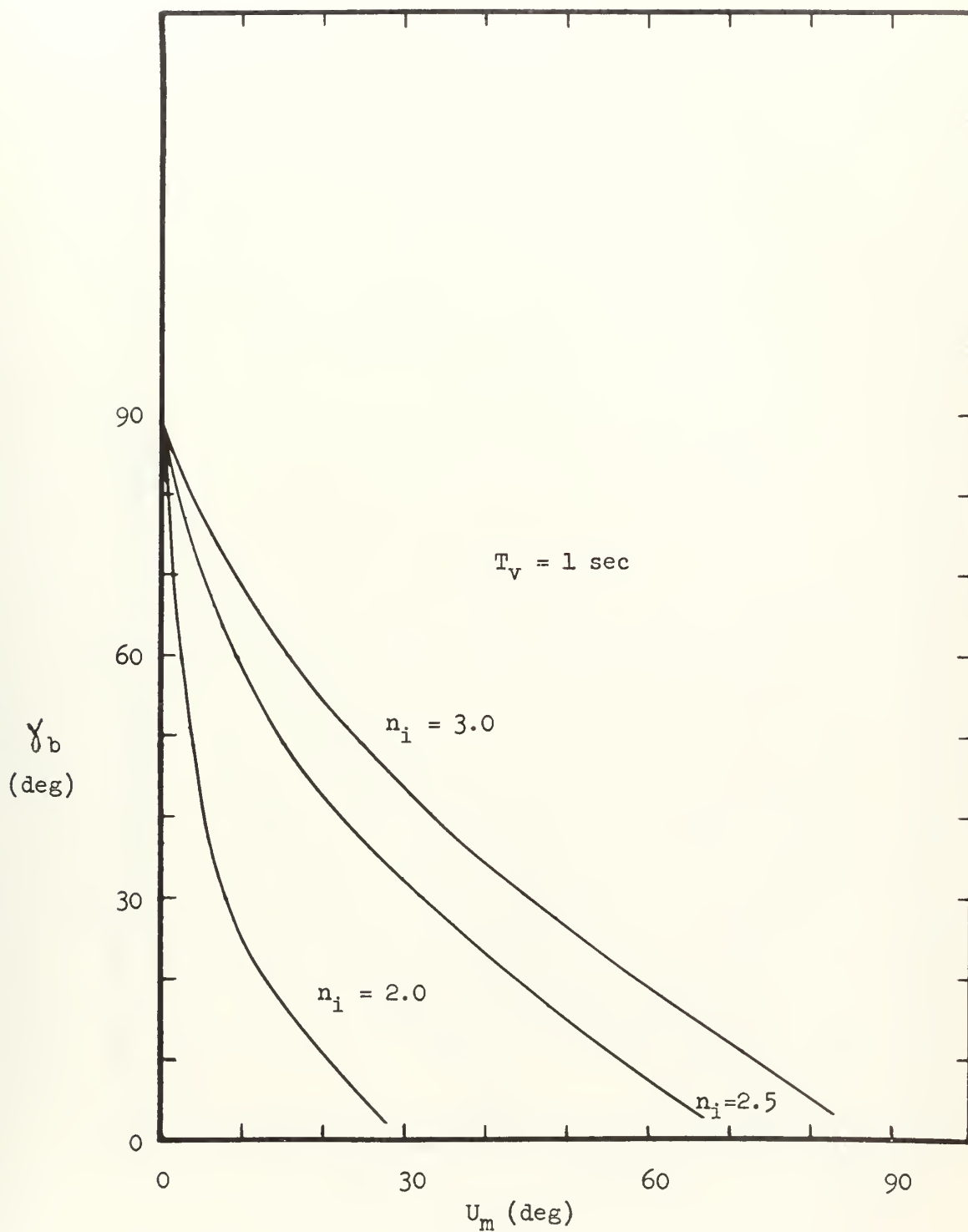
Fig. 15   Variation of γ_b with U_m for various values of n_i at a T_v of 1 second.
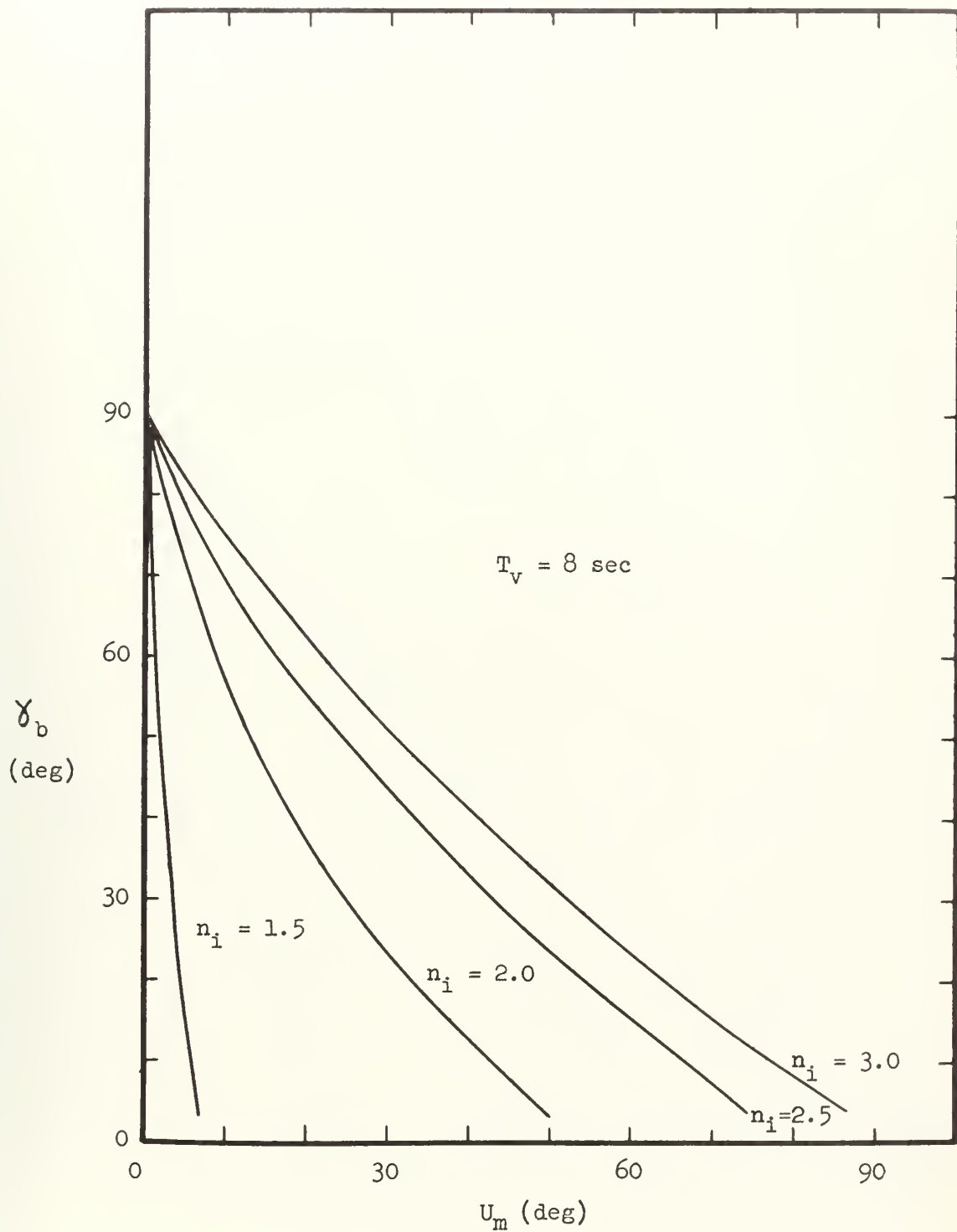
Fig. 16   Variation of γ_b with U_m for various values of n_i at a T_v of 8 seconds.
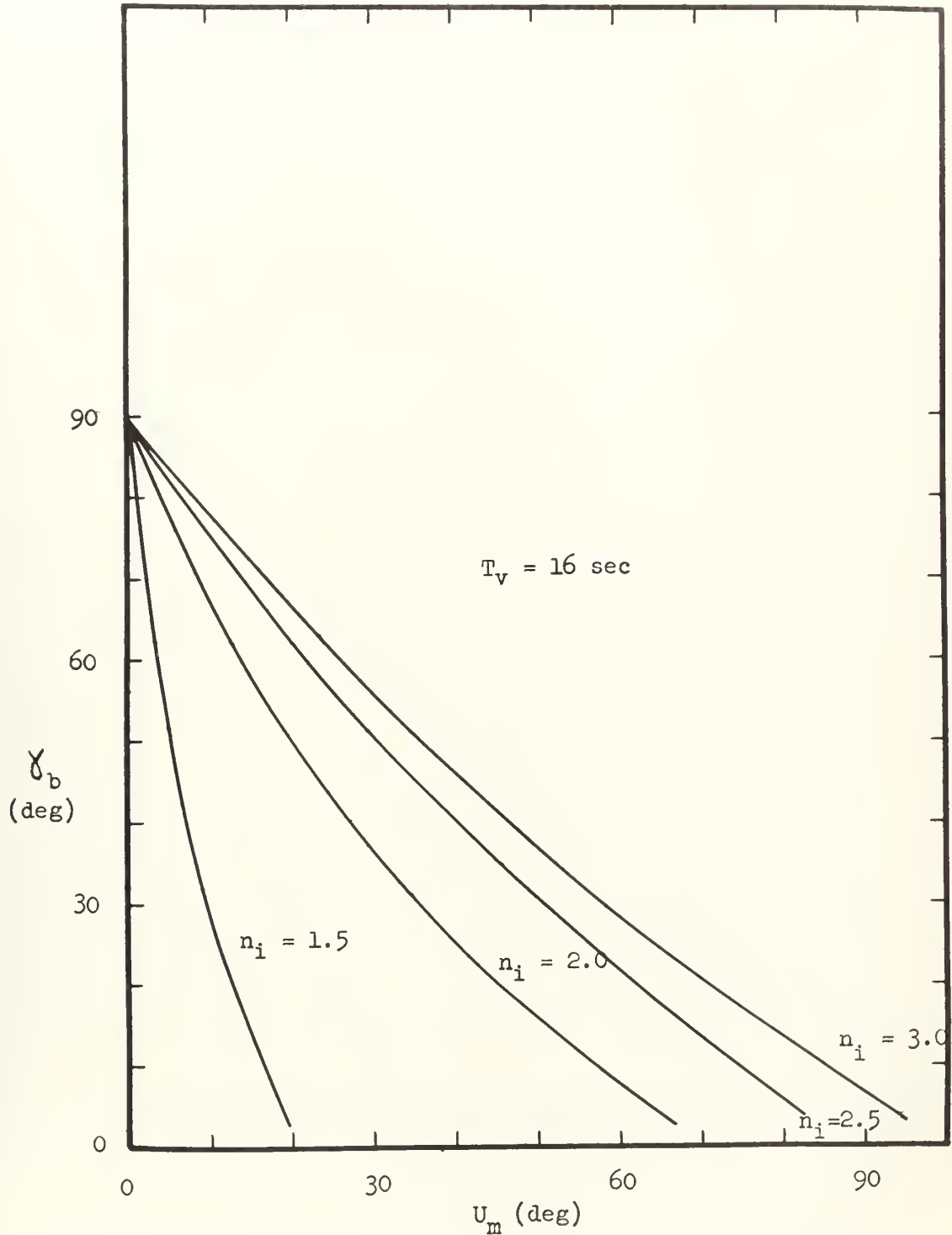
Fig. 17   Variation of γ_b with U_m for various values of n_i at a T_v of 16 seconds.

Fig. 18   Variation of γ_b with U_m for various values of n_i at a T_v of 24 seconds.

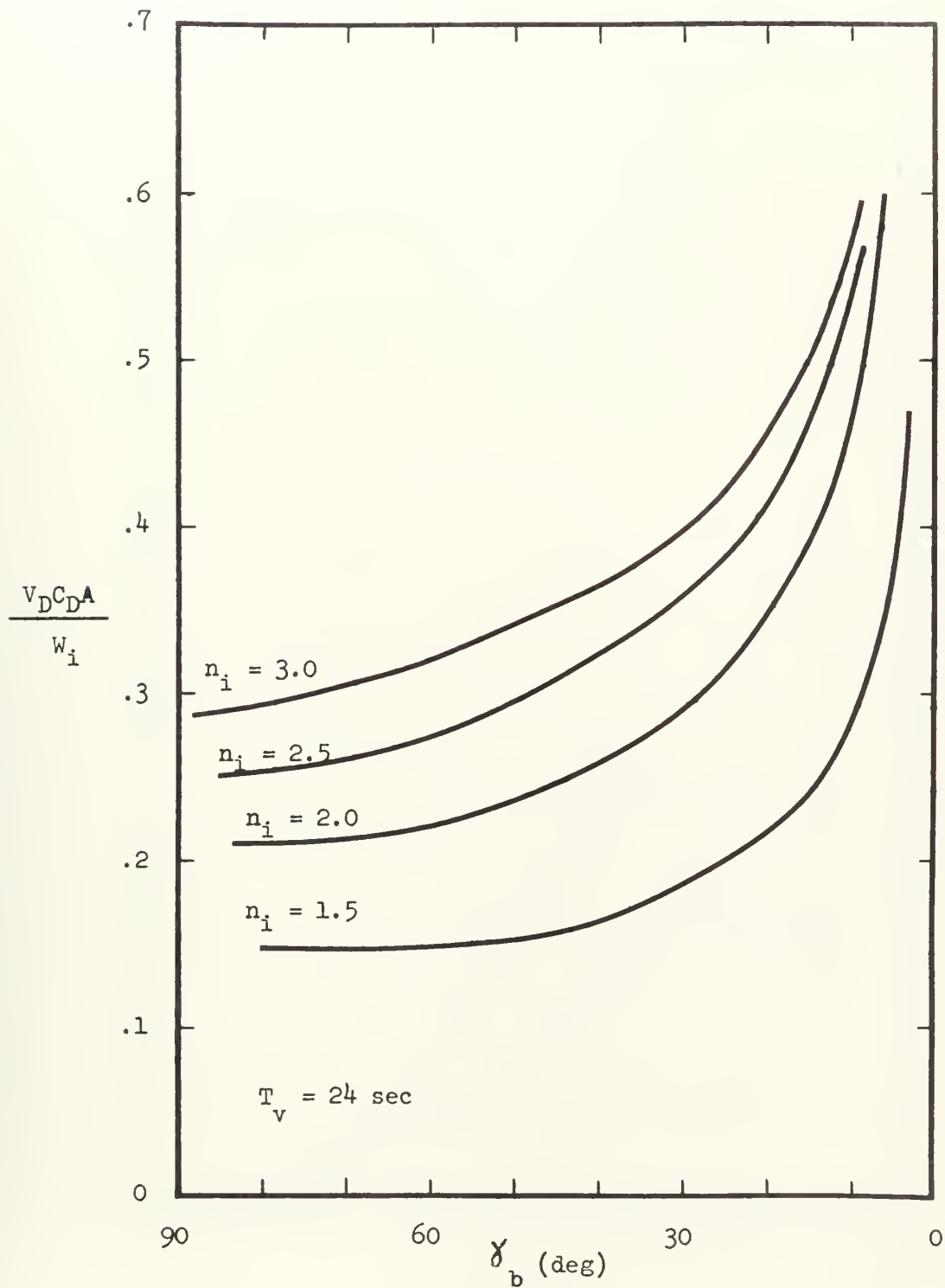Fig. 19   Drag velocity loss as a function of γ_b for various values of n_i at a T_V of 1 second.
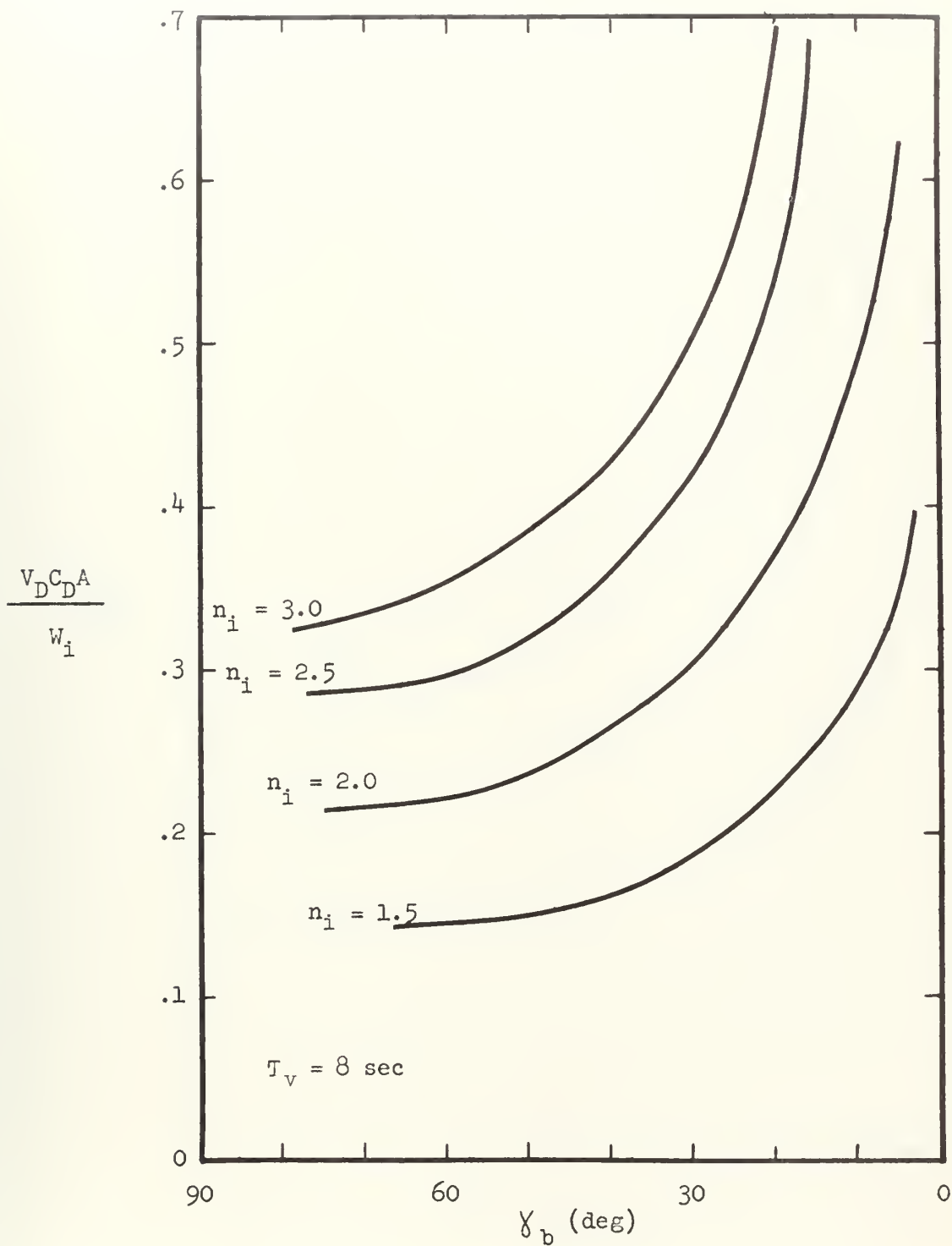
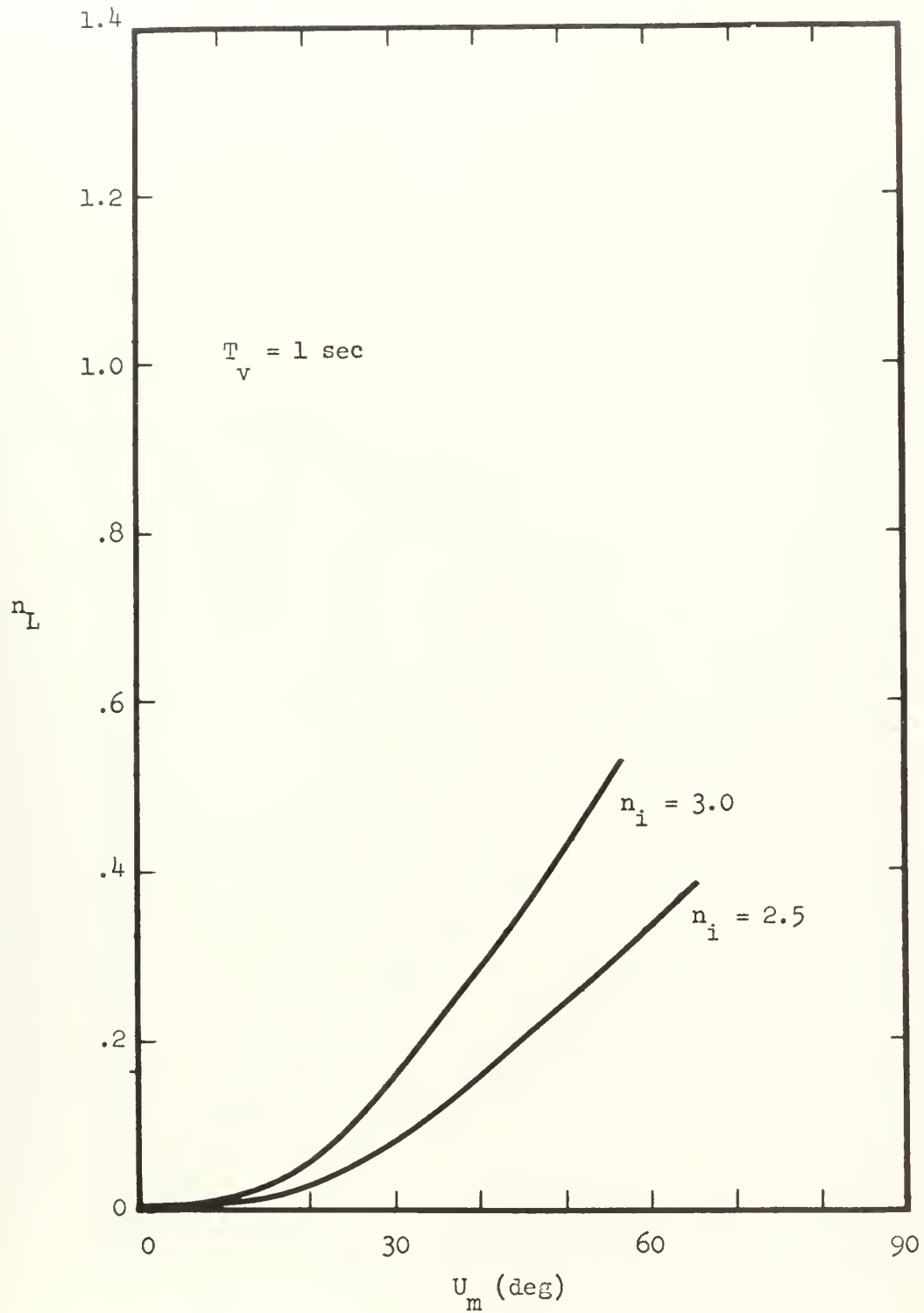Fig. 20 Drag velocity loss as a function of γ_b for various values of n_i at a T_v of 8 seconds.
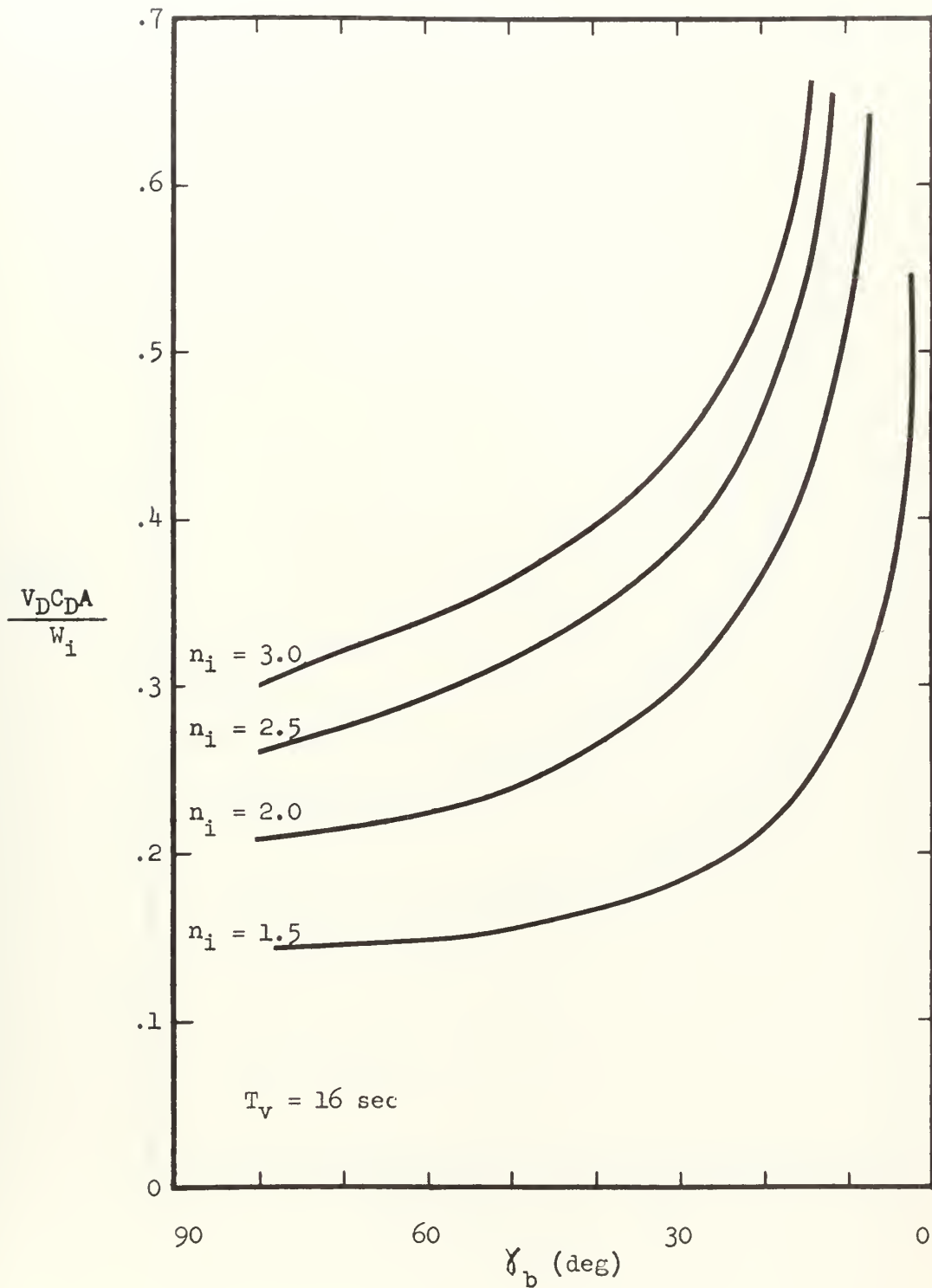
Fig. 21 Drag velocity loss as a function of γ_b for various values of n_i at a T_v of 16 seconds.

Fig. 22 Drag velocity loss as a function of γ_b for various
values of n_i at a T_v of 24 seconds.

Fig. 23   Variation of maximum lift load factor with U_m for various
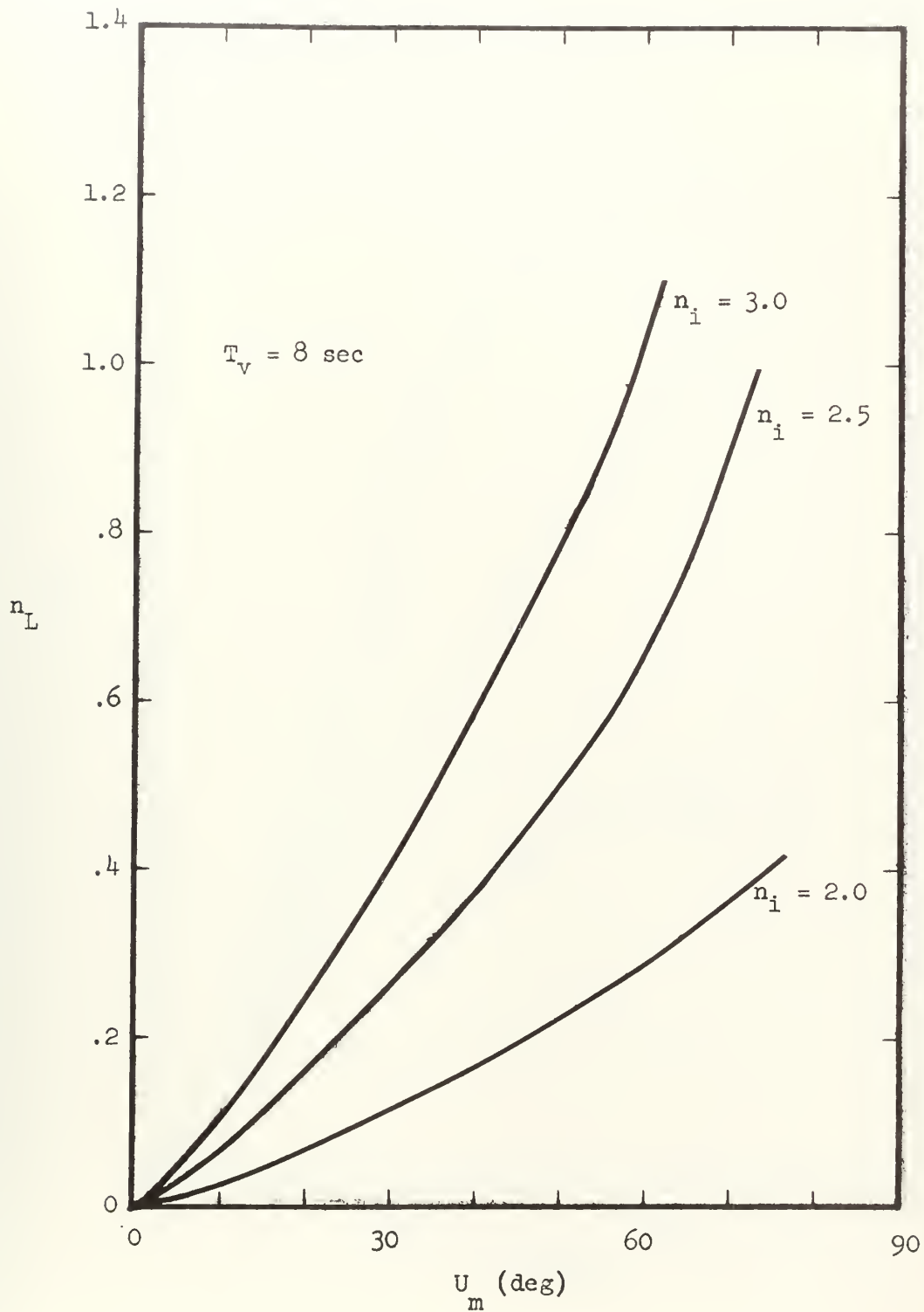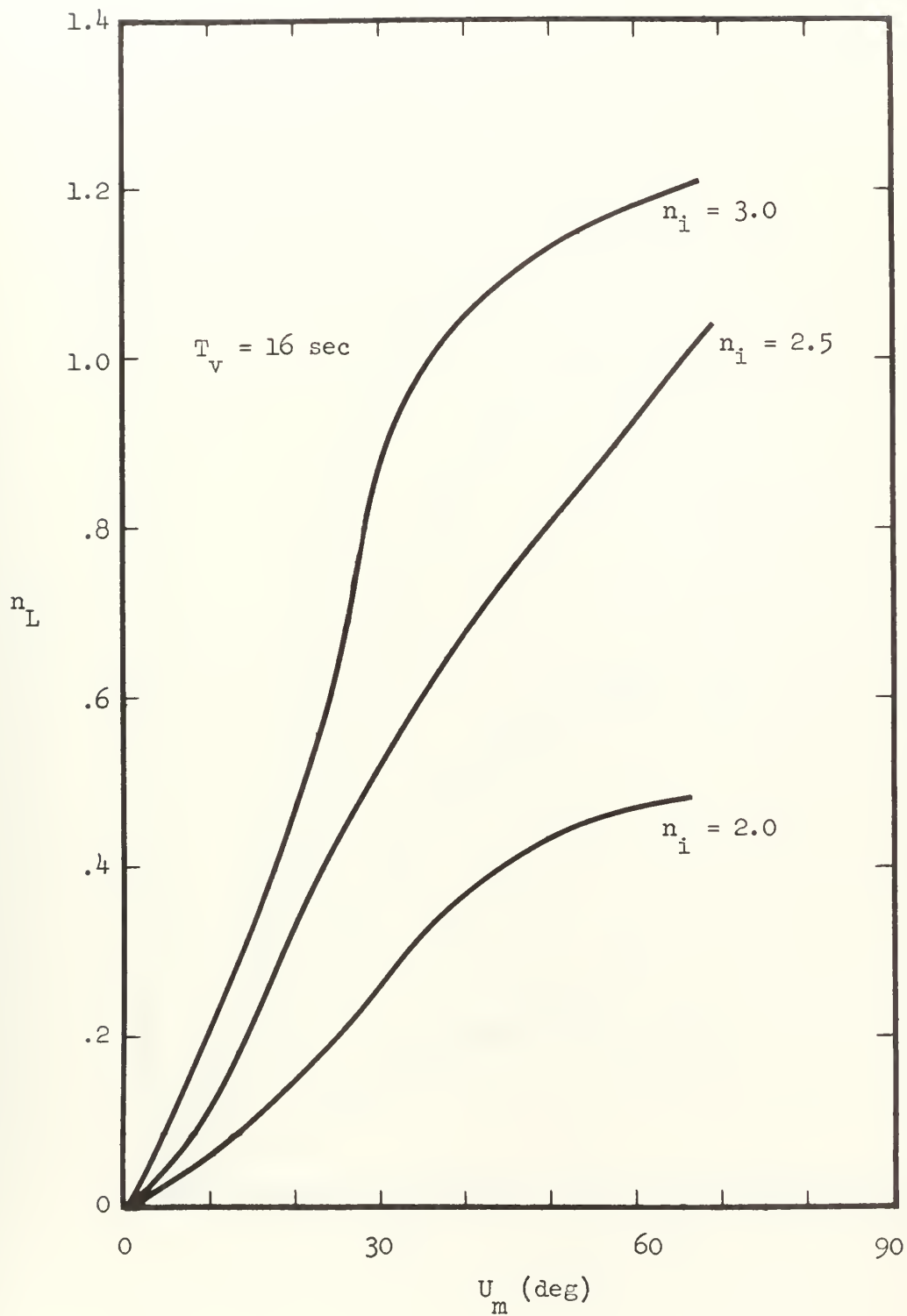values of n_i at a T_v of 8 seconds.

Fig. 24   Variation of maximum lift load factor with U_m for various
values of n_i at a T_v of 8 seconds.

Fig. 25   Variation of maximum lift load factor with U_m for various values of n_i at a T_v of 16 seconds.
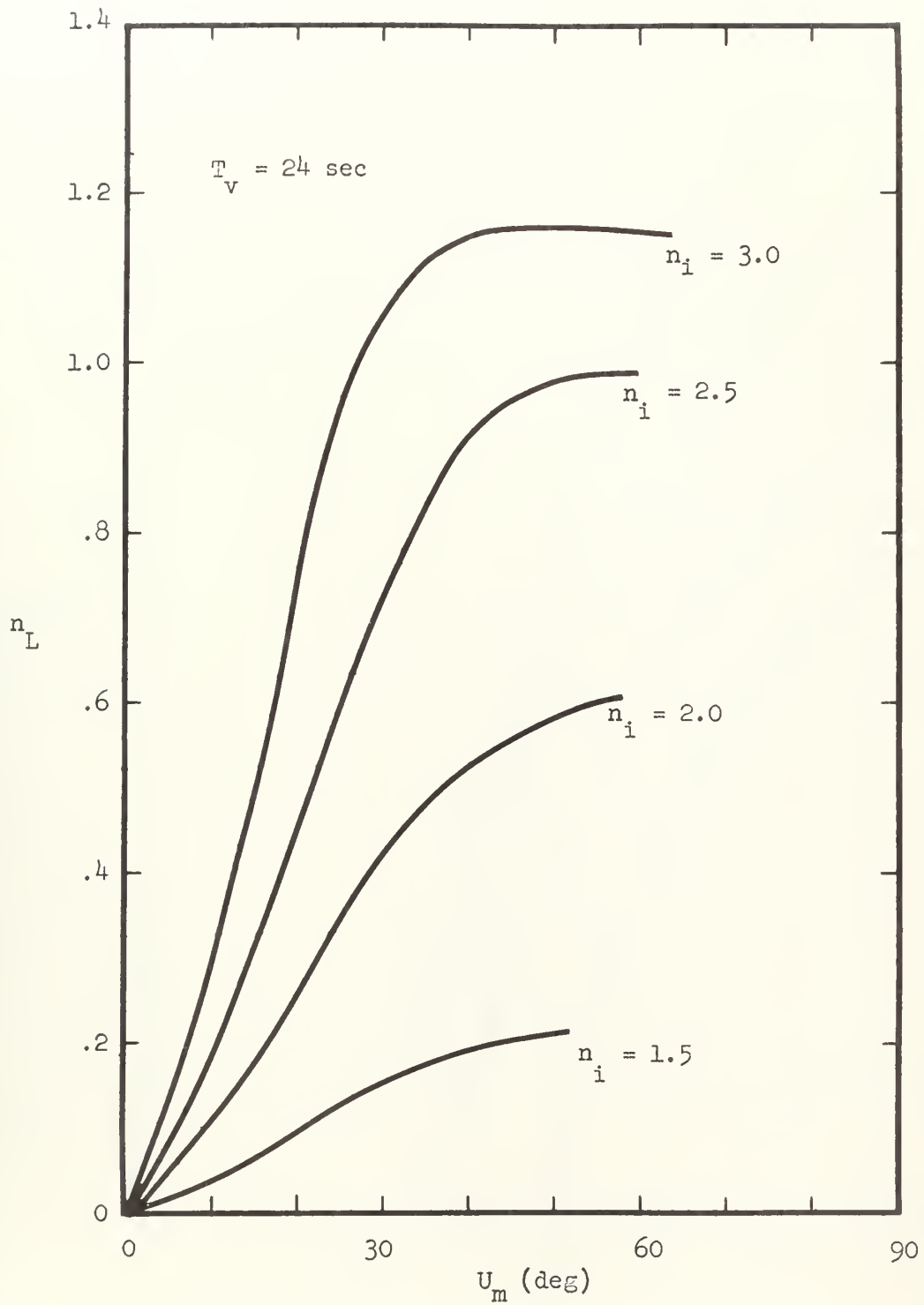
Fig. 26   Variation of maximum lift load factor with U_m for various values of n_i at a T_v of 24 seconds.
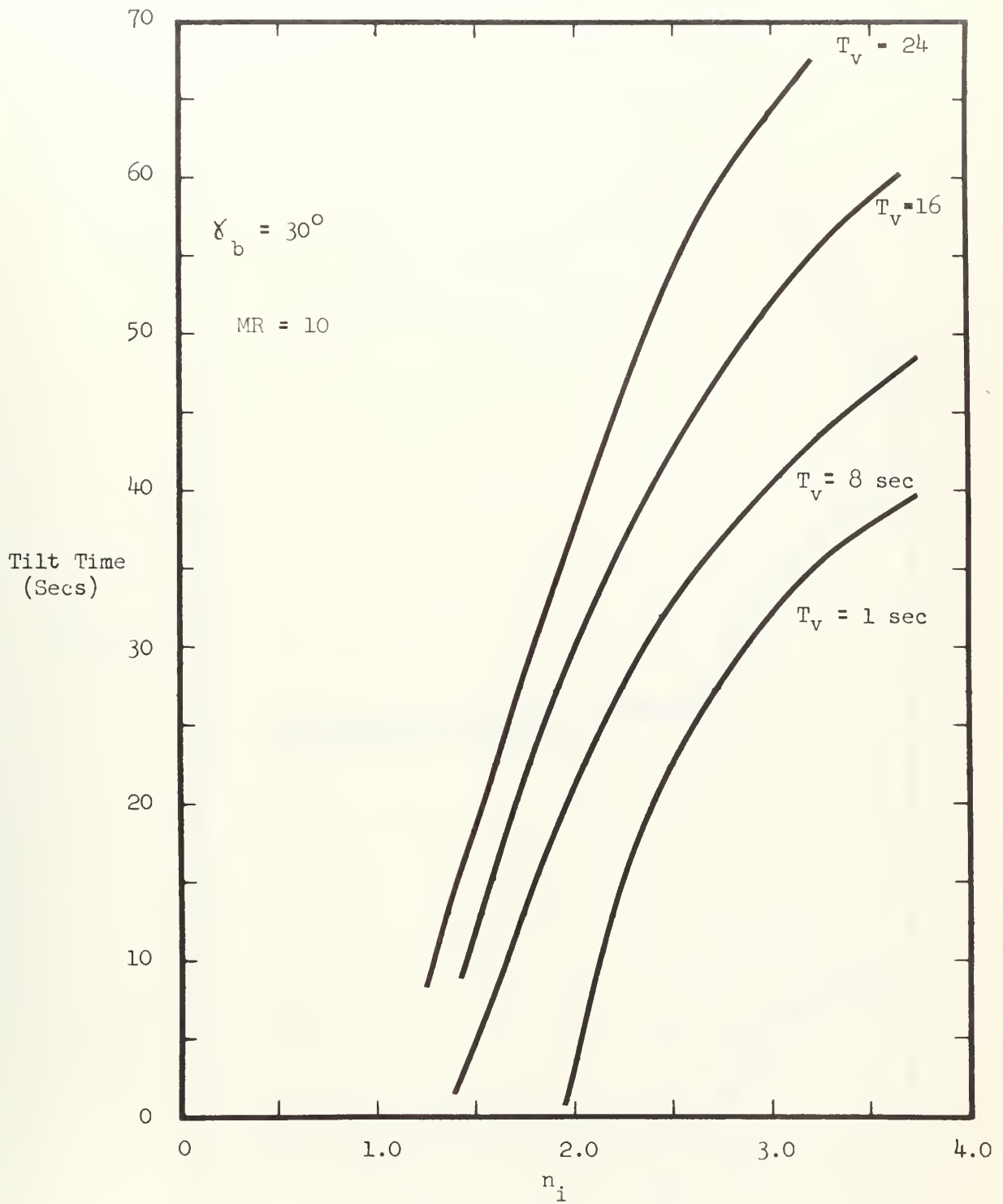
Fig. 27   Variation of tilting time with n_i for various values of T_v to reach a γ_b of $30°$.
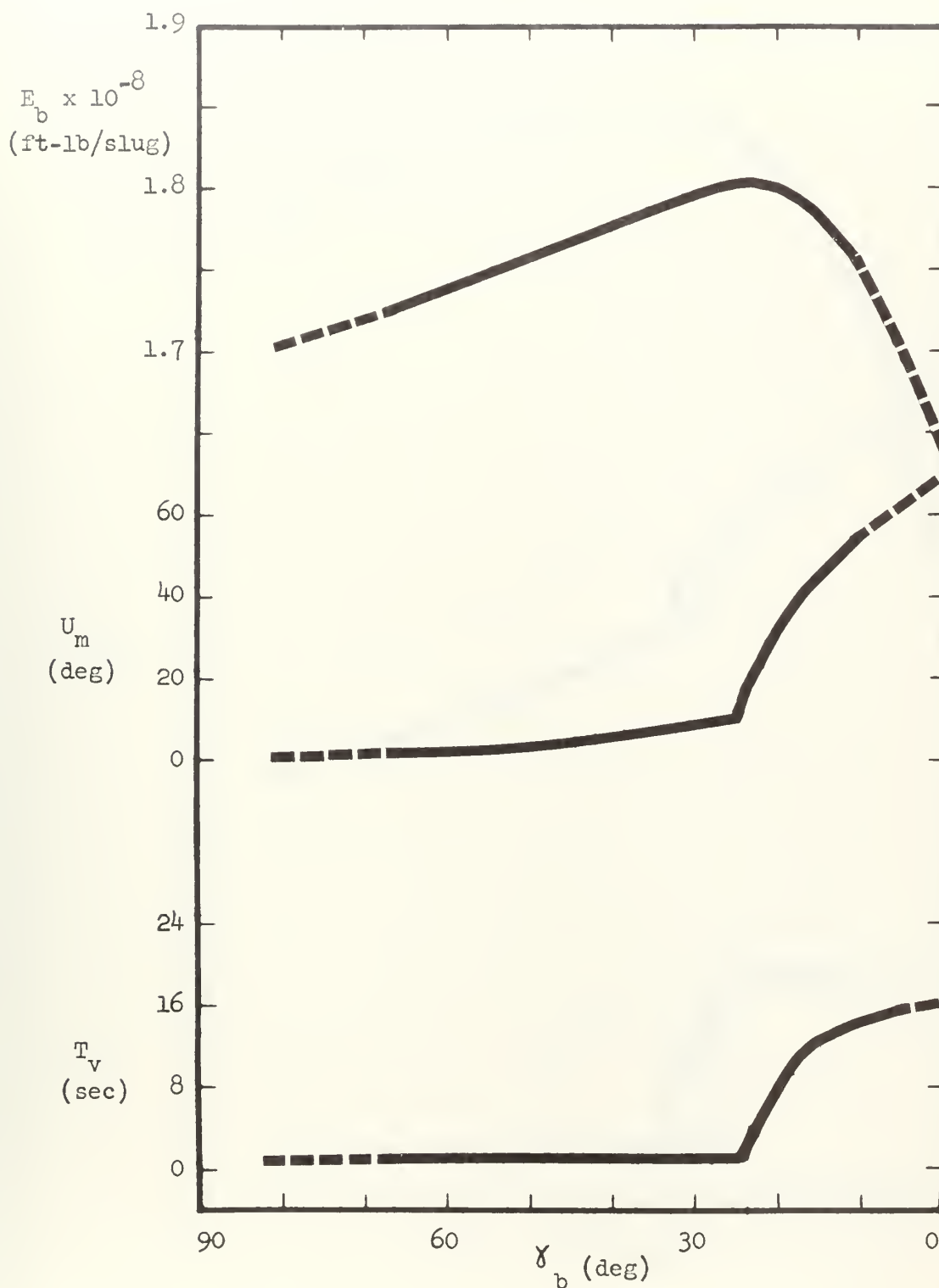
Fig. 28   Values of U_m and T_v required to obtain a specified γ_b
under maximum energy conditions for n_i of 2.0.
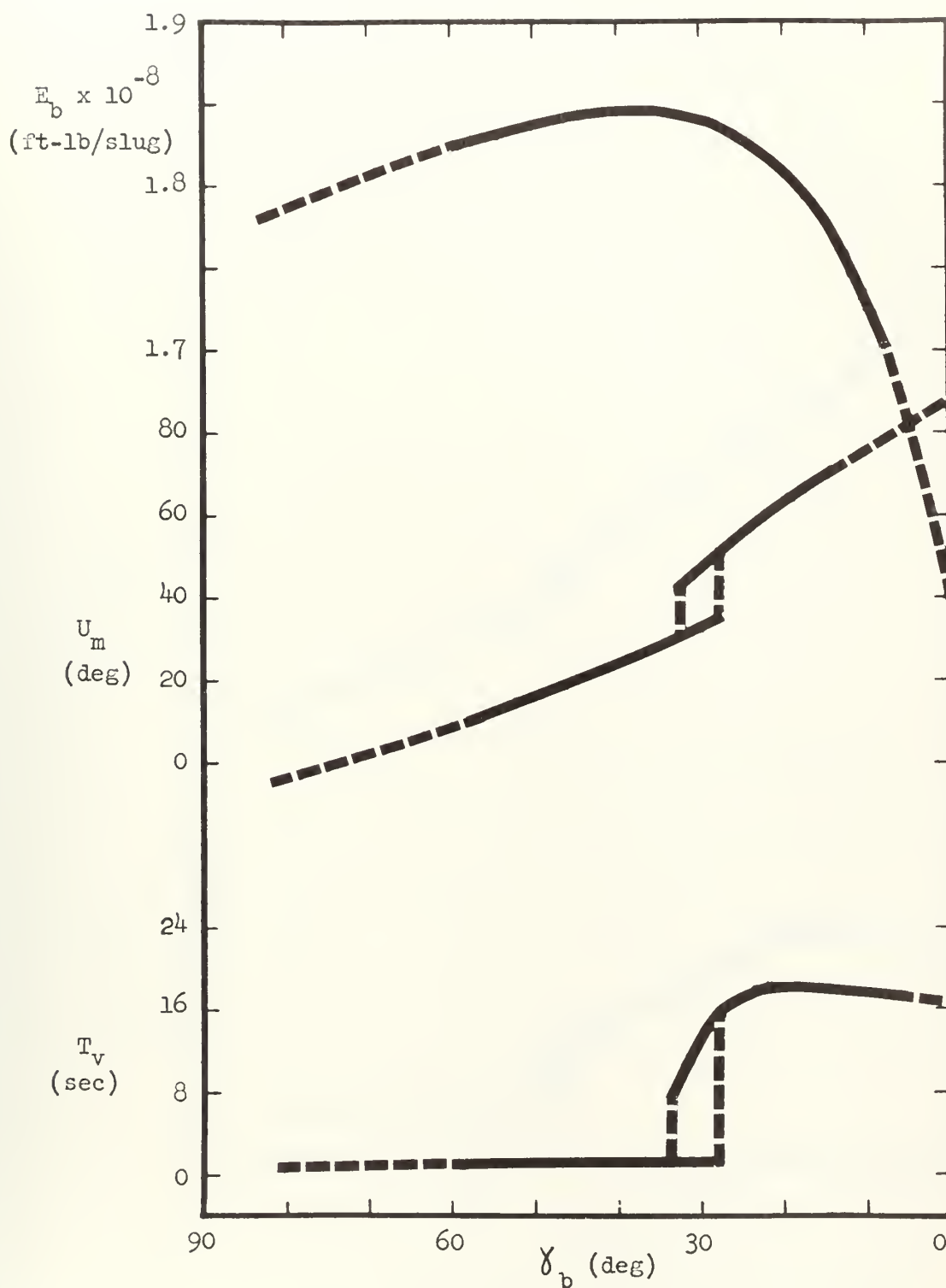
Fig. 29   Values of U_m and T_v required to obtain a specified γ_b
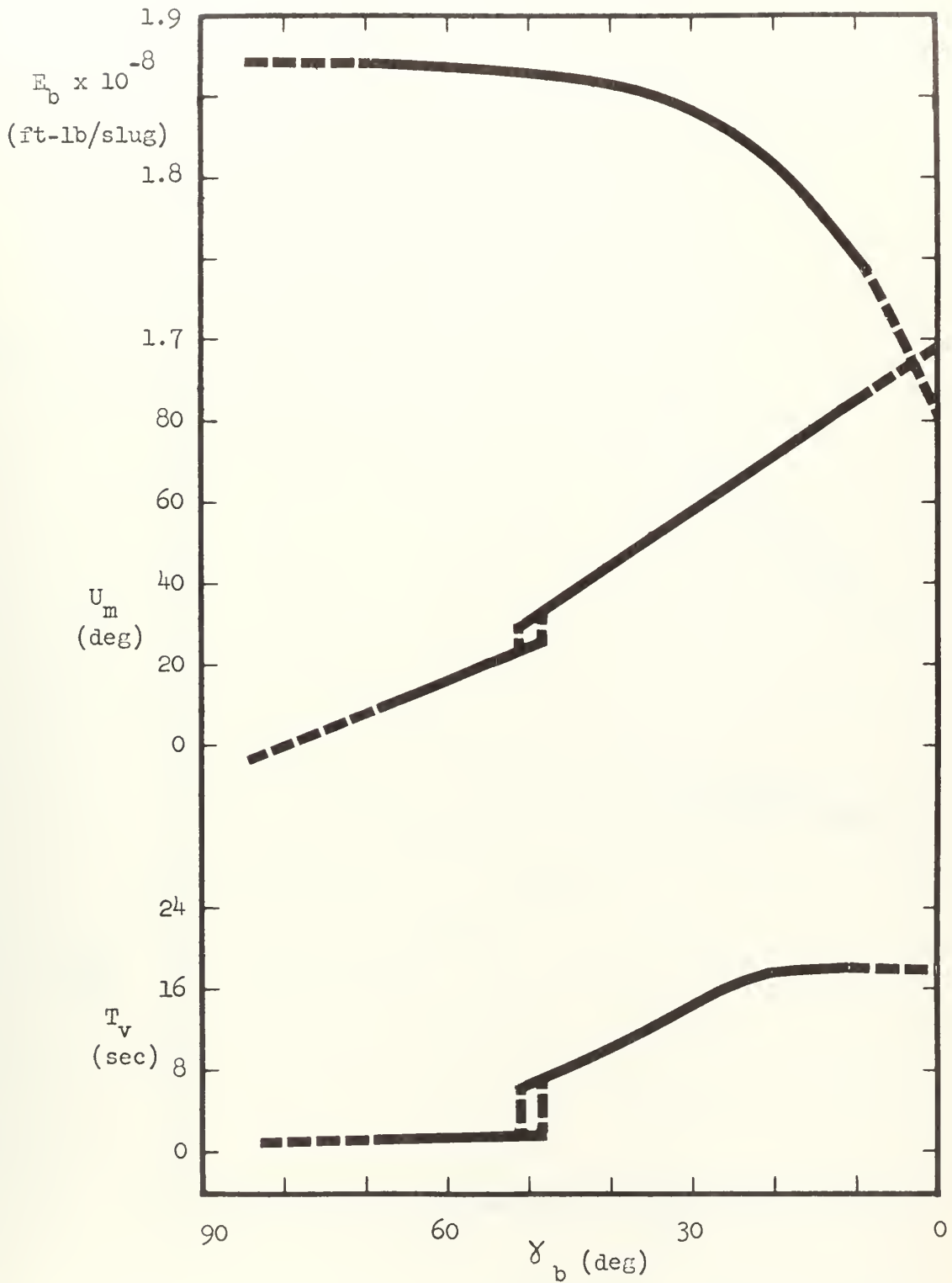under maximum energy conditions for n_i of 2.5.

Fig. 30 Values of U_m and T_v required to obtain a specified γ_b under maximum energy conditions for n_i of 3.0.
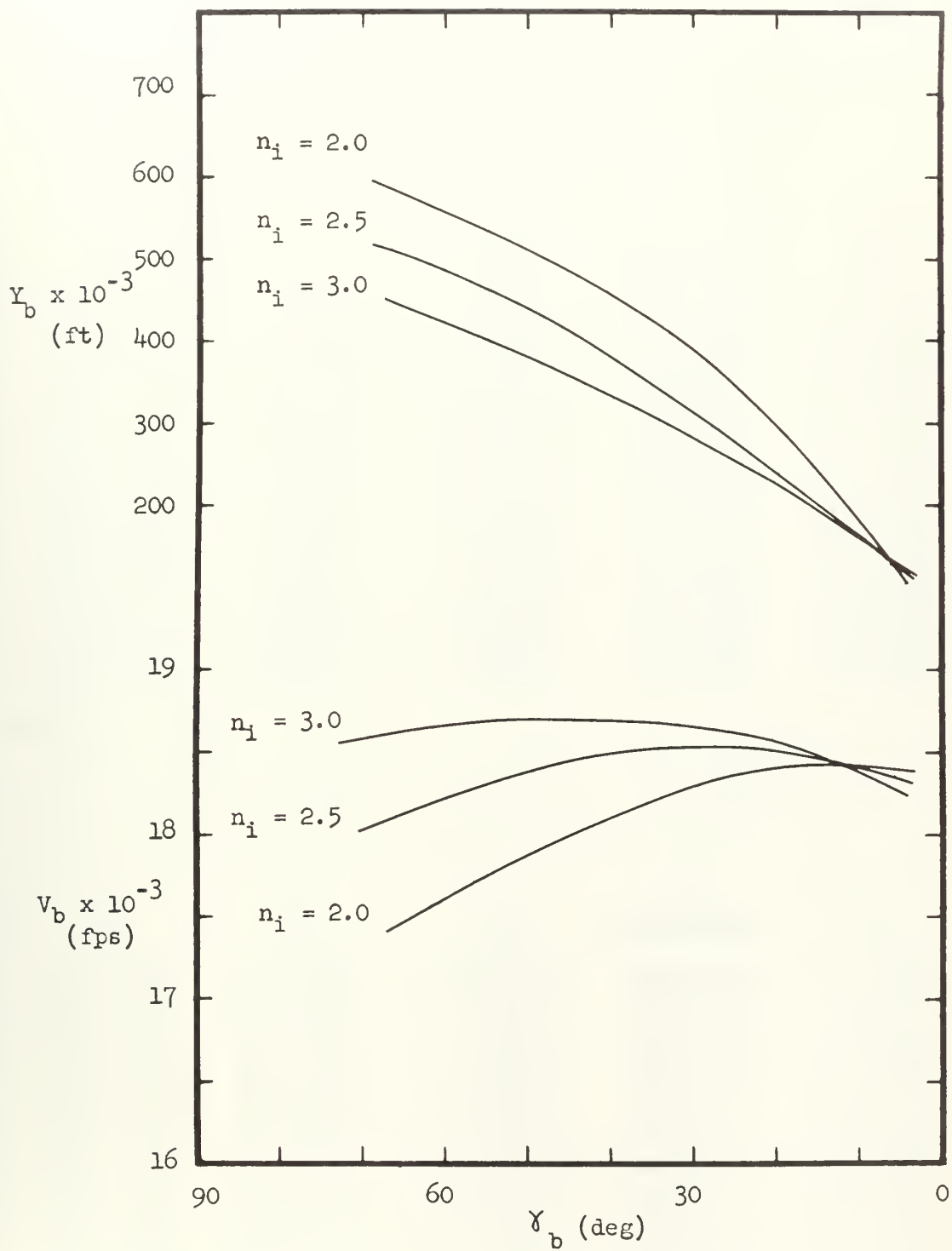
Fig. 31   Values of Y_b and V_b at maximum energy.

TABLE V

COMPUTER RESULTS FOR REPRESENTATIVE TRAJECTORIES

A. $n_i = 3.0$ $T_v = 1$ sec $U_m = 20^o$

T sec	V fps	Y ft	γ deg	E ft-lb/slug	V_D fps
4	265.78352	525.70761	87.002181	52234.583	.20644683
8	546.99767	2129.7715	80.949374	218126.61	2.2177488
16	1152.0408	8609.4335	70.776125	940599.34	27.850098
17*	1227.7526	9726.6649	70.160493	1066634.4	37.685454
21	1535.2739	14867.757	69.635561	1656889.0	87.560342
29	2087.3356	28129.005	66.455353	3083509.0	331.30749
37	2731.9199	45316.107	63.757048	5189695.9	610.93239
45	3626.1614	67522.151	61.496942	8746984.1	802.44887
53	4799.5585	96429.217	59.667247	14620399.0	925.23353
61	6325.6918	134027.09	58.208353	24319383.0	982.43218
69	8308.6788	182846.45	57.055556	40399983.0	1000.4780
77	10972.134	246406.84	56.151720	68121766.0	1005.5098
85	14886.326	330622.30	55.454918	121438810	1006.2890
90	18668.867	398806.33	54.922312	187094520	1006.2980

* End of tilt phase.

B. $n_i = 2.5$ $T_v = 1$ sec $U_m = 26^o$

T sec	V fps	Y ft	γ deg	E ft-lb/slug	V_D fps
4	199.15440	393.99420	86.681749	32507.627	.11541601
8	409.79788	1593.1459	80.054237	135225.11	1.2274019
12	632.93575	3600.1614	73.392714	316135.60	4.6832111
16	870.24830	6387.4618	66.923305	584176.57	11.738844
18*	992.92178	8071.9079	64.713429	752652.80	18.598280
22	1244.3838	12031.649	63.844218	1161352.4	39.663503
30	1705.8846	2213.8303	58.869145	2167300.1	180.90261
38	2151.1125	34644.219	54.543873	3428287.3	425.59583
46	2721.8130	49616.932	50.715587	5300510.7	647.48641
54	3476.8072	67782.124	47.445993	8224919.4	808.12281
62	4427.3496	89914.139	44.721666	12693614.0	924.52635
70	5617.1983	116914.58	42.479115	19538075.0	994.29298
78	7100.7933	149892.68	40.646909	30033288.0	1026.7656
86	8964.8019	190264.90	39.157532	46305429.0	1040.6460
94	11391.601	240036.72	37.954541	72607238.0	1045.6924
102	14785.568	302500.64	36.996442	119039180	1047.0206
108	18585.407	361322.79	36.152776	184333900	1047.0806

* End of tilt phase.

TABLE V (Continued)

C. n_i = 1.5 T_v = 16 sec U_m = 18°

T sec	V fps	Y ft	γ deg	E ft-lb/slug	V_D fps
4	67.000877	132.68853	89.999999	6513.6862	
8	137.96242	541.24719	89.999999	26930.929	.060251961
12	212.91698	1241.5799	89.999999	62613.474	.31773094
16	291.88676	2249.6993	89.999999	114980.88	.93047546
20	374.09575	3580.1953	88.110768	185163.20	2.3827188
24	459.54522	5236.3599	82.724083	274065.82	4.8911670
28	551.81331	7208.5201	76.258076	384176.26	8.2929824
31*	626.59842	8900.2976	72.774338	482671.41	11.335807
35	732.62606	11454.434	71.827600	636906.00	15.982745
43	964.12244	17603.648	65.552245	1031146.7	31.150525
51	1207.2451	25045.312	59.270032	1534529.5	72.764797
59	1450.8226	33523.212	53.090988	2131020.6	157.13915
67	1706.2258	42720.706	47.055876	2830101.4	278.08037
75	2027.7450	52525.718	41.291939	3745840.0	386.30959
83	2423.2376	62935.490	35.985004	4960929.9	478.66841
91	2898.4151	73921.632	31.228459	6578763.4	554.25915
99	3452.0813	85422.589	27.038602	8706823.1	619.84834
107	4089.9748	97349.100	23.380049	11496062.0	676.75458
115	4821.4522	109613.97	20.200540	15149926.0	724.96740
123	5658.5944	122137.53	17.444041	19939505.0	765.06602
131	6621.16994	134856.15	15.057469	26262321.0	794.20610
135	7154.6835	141271.78	13.987885	30140033.0	807.78328
147	9009.8838	160685.28	11.208726	45758899.0	844.95417
155	10523.848	173759.37	9.6691722	60966233.0	867.32021
163	12354.673	186986.81	8.3463049	82335093.0	888.65247
171	14652.533	200490.62	7.2179499	11379896.0	910.07619
180	18181.017	216305.47	5.8239900	17223411.0	936.87476

* End of tilt phase.

TABLE V (Continued)

D. $n_i = \overset{2.0}{\cancel{1.5}}$ $T_v = \overset{1}{\cancel{16}}$ sec $U_m = \overset{12°}{\cancel{18°}}$

T sec	V fps	Y ft	γ deg	E ft-lb/slug	V_D fps
4	132.98571	262.85677	86.04007	17299.766	.051083963
8*	274.54739	1061.2315	78.231773	71832.250	.53748828
12	425.70506	2406.9641	76.811880	168054.18	1.5548419
20	755.87968	6784.9449	69.191874	503976.21	8.4062369
28	1118.9996	13404.599	62.519935	1057360.3	31.113584
36	1473.1912	22048.882	56.628937	1794548.0	117.69074
44	1797.8701	32228.993	51.247801	2653105.7	295.59529
52	2184.0412	43659.480	46.242080	3789720.3	481.84897
60	2687.6234	56560.978	41.736274	5431455.5	629.68643
68	3312.1204	71204.977	37.809023	7776023.5	746.65796
76	4064.6675	87822.151	34.444157	11086355.0	840.03946
84	4967.0819	106668.91	31.587084	15767923.0	907.74155
92	6045.2513	128059.42	29.174504	22392722.0	951.86607
100	7336.8161	152389.86	27.144237	31817434.0	976.00713
108	8894.5880	180171.00	25.440375	45353679.0	991.09169
116	10821.625	212127.15	24.016065	65378775.0	999.40505
124	13307.439	249378.99	22.835027	96567497.0	1003.5360
132	16759.873	293825.31	21.546874	149900220.	1005.0832
135	18484.668	312997.36	21.250934	180911870.	1005.2250

* End of tilt phase.

CHAPTER 7

DISCUSSION OF RESULTS

The status of the vehicle at burnout is of prime importance. This vehicle status is best described by the burnout quantities, V_b, Y_b, E_b, and γ_b, as displayed in Figs. 5 through 18.

These burnout values are not shown for the vehicle where the value of n_i is 1.5 and the T_v is 1 second, due to the fact that the vehicle passes through the horizontal and heads back towards the earth before reaching burnout. This result is readily explained since the vehicle is relatively slow and turns at a low altitude where drag losses are very large.

The vehicle does reach burnout conditions for the other values of T_v, however. For the case where n_i is 1.5, the value of V_b peaks at a very low value of U_m. The larger values of U_m cause the relatively slow vehicle to turn more at a low altitude. This reduces V_b due to the fact that the vehicle operates for a longer period in dense atmosphere where the drag velocity loss is very large.

As T_v is increased, the maximum value of V_b obtained for an n_i of 1.5 occurs at the higher values of U_m. This happens as a result of the in-creased velocity and the higher altitude reached before the tilting is commenced. Drag velocity loss is much less under these circumstances. It is true that gravity velocity loss increases as T_v is increased but it does not offset the reduction of the velocity loss due to drag. This fact is

further borne out by observing that the curves indicate higher burnout altitudes are reached as the value of U_m is reduced.

The burnout altitude reached varies inversely with the value of U_m and directly with the value of T_v for the vehicle with an n_i of 1.5. Both of these phenomena are readily explained since the altitude attained is a direct function of the vertical component of the velocity vector which is directly affected by these two factors.

The value of γ_b of the vehicle for the values of n_i = 1.5 generally decreases with increased values of U_m and with an increase in T_v. A large U_m allows a greater amount of turn of the vehicle, hence a smaller γ_b. At the higher values of T_v the vehicle has a greater velocity before commencing the turn, and hence does not get turned as much since the gravity vector causing the turn after U_m is reached is small in comparison to the vertical component of the velocity vector of the vehicle.

Generally, the burnout energy of the vehicle follows the trend of the velocity at burnout. This is explained by the fact that energy is directly proportional to the square of the velocity.

As the value of n_i is increased the burnout velocity attained becomes less and less dependent upon the value of U_m, which is indicated by the fact that the curves of V_b versus U_m tend to flatten out as the value of n_i increases. Vertical flight time does not affect the burnout velocity to any great degree and at higher vertical flight times the value of U_m appears to have less affect on the V_b reached. The basic reason for these effects is that with a high n_i and T_v the vehicle is out of the very dense atmosphere before turning, and hence the drag velocity loss is relatively small.

As n_i is increased the burnout altitudes become less and less at the low values of U_m and just slightly more at the high values of U_m. At

the higher values of U_m the high n_i vehicle does not get turned as much as the lower n_i vehicle and hence attains a slightly higher burnout altitude.

Vertical flight time seems to have little effect on the burnout velocity attained. It appears to be a slight factor at low values of T_v, but for values of T_v greater than 8 seconds, vertical flight time has no appreciable effect upon the burnout velocity reached. The value of γ_b decreases with an increase in n_i for the reasons previously explained.

The drag velocity loss of the missile for the various trajectories studied is shown in Figs. 24 through 27. The variation of this loss with γ_b and n_i for four values of T_v is shown. The more prominent indications of these results are:

(1)   High n_i missiles have the highest drag velocity loss.

(2)   The drag velocity losses decrease slightly with an increase in vertical flight time.

(3)   Drag velocity losses greatly increase as the missile attitude approaches the horizontal at burnout.

The higher drag velocity losses accompanying an increase in the value of n_i is a result of the higher velocities attained by the vehicle at lower altitudes. Since drag force is directly proportional to the square of the velocity and to the density of the atmosphere, this force, and hence the resulting velocity loss, is large for a high n_i missile. Since the drag velocity loss may be expressed as:

$$V_D = g_o \int \frac{D}{W}\, dt$$

it must be realized that a slow, large vehicle would experience a lower drag velocity loss than would a smaller, faster missile.

The drag velocity loss decreases slightly with an increase in vertical flight time because the missile is at a higher altitude and hence in a less dense atmosphere before it commences to turn. It therefore spends less time in the denser atmosphere of low altitudes. This decrease in drag velocity loss as indicated in the aforementioned plots, is not as great as would be expected. The drag loss is plotted versus γ_b, and to get to the same value of γ_b for a high vertical flight time as for a low vertical flight time, the vehicle must be turning at an angle of attack for a longer period of time since the missile has a greater velocity at the start of the tilting phase. This increased time of tilt with an angle of attack increases the drag coefficient due to the induced drag present while this condition exists.

Nearly the same reasoning applies to the condition of increased drag velocity loss for a smaller value of γ_b attained for a particular vehicle with a given n_i at a certain T_v. The smaller value of γ_b requires that the missile be tilted at an angle of attack for a longer period and hence the drag coefficient is again increased.

The values of n_L which are plotted against U_m in Figs. 28 through 31 show the maximum negative lift load factor encountered during a trajectory of specified T_v and U_m. Lift is always negative in the tilt phase, that is, in the direction of rotation of the vehicle. Lift load factor increases rapidly with increased U_m for the high n_i trajectories. The slope of the lift load factor curve increases as T_v is increased, as could be expected from the higher dynamic pressures caused by the higher velocities associated with long vertical flight times. An interesting aspect of the higher T_v plots is that the maximum n_L seems to level off, reaching a maximum of about 1.2 g's for an n_i of 3.0. In these cases the missile has reached the less

dense portions of the atmosphere, where the extremely low density has offset
the increased velocity, and the maximum n_L encountered has become essentially
constant. The large values of n_L encountered for high n_i trajectories and
the accompanying bending moments are too great for most contemporary liquid
fueled vehicles. Use of trajectories of this nature require the heavier
structural design associated with solid fueled vehicles.

It might be mentioned at this point that the rate of tilt should
have a considerable affect on lift. This program uses a tilting rate of two
degrees per second, which is considered a nominal rate for a large rocket-
powered vehicle control system to achieve, but a minimum rate to reach the
maximum programmed tilt angle within a reasonable time. The two degree per
second tilt rate was selected to keep the lift load factor within practical
bounds. A study of methods for obtaining minimum lift loads through differ-
ent types of tilting programs is of interest, but beyond the purposes of
this paper.

The variation of tilt time necessary to reach a γ_b of 30° for
four different vertical flight times is plotted against n_i in Fig. 27. The
curves indicate that the tilt time increases as both T_v and n_i increases.

The higher the value of T_v used, the greater the velocity of the
vehicle becomes before the vehicle starts to turn. Since this is the case,
it takes much longer to turn the vehicle from the vertical position to a γ_b
of 30° at the higher value of T_v than at the lower values. This same type
of reasoning may also be applied to the second observation, in that at high
values of n_i the vehicle gains greater velocities sooner than at low values
of n_i. It therefore requires a greater tilt time to reach a γ_b of 30° at
the higher values of n_i.

The optimization program undertaken in this paper is based on maximum specific energy. The combination of T_v and U_m which would give maximum burnout energy for a specified burnout angle are determined. Energy is maximized in this manner for the three higher values of n_i. The resulting values of E_b, U_m and T_v are plotted versus burnout angle in Figs. 19 through 21. It is not possible to obtain a good optimization for an n_i of 1.5 with the data available. At this value of n_i, burnout energy is extremely sensitive to T_v and U_m, and any attempt at optimization requires a large number of trajectories. Accordingly, no optimization is included for an n_i of 1.5.

Good maximum energy points are found for burnout angles below about thirty degrees. In the range of thirty to fifty degrees, two approximately equal maximum energy points appear. One of these points occurs at a value of T_v consistent with the maximum points found in the thirty degree and below range, while the other occurs at the minimum T_v, which is one second. Above the thirty to fifty degree range the maximum energy points are found at the minimum values of T_v and U_m for the particular burnout angle. These same characteristics, in varying degree, are found for each value of n_i. The overlapping in the plots of T_v and U_m versus burnout angle in the thirty to fifty degree range show that in this area maximum energy can be obtained by using either of two combinations of T_v and U_m. This effect is undoubtedly caused by the non-linear action of drag on the trajectories. A point is reached for each n_i where the beneficial effects of early tilting, and consequent earlier alignment of thrust and velocity vectors in the desired direction, are overcome by the higher drag losses associated with large programmed tilt angles at low altitudes. At this point it is necessary to use a period of vertical flight time to get the vehicle out of the denser portions of the atmosphere during the tilting maneuver.

The amount of vertical flight time required to maximize burnout energy for low burnout angles does not increase indefinitely as burnout angle approaches zero, but tends to level off in the neighborhood of 16 to 20 seconds. This is especially evident in Fig. 21 where n_i is 3.0. The high velocity reached at the end of a long vertical flight time causes an increased negative lift load during the tilting phase, which increases the drag coefficient, thereby reducing burnout velocity and burnout energy.

It is interesting to note that at burnout angles of about ten degrees and below, the maximum burnout energies for all three values of n_i fall very close together. This indicates that for very low burnout angles the advantage of a high initial acceleration rocket is questionable, since the same burnout energy can be obtained using a lower initial acceleration with lower aerodynamic loads. At other values of burnout angle the higher burnout energies obtained from high n_i rockets are apparent. The point at which maximum overall burnout energy is reached starts at a burnout angle in the vicinity of twenty-five degrees for an n_i of 2.0, and moves in the direction of increasing burnout angle as n_i increases. In this case, the increased drag associated with high initial acceleration and low burnout angle causes the maximum overall energy points to fall at higher burnout angles for the higher values of n_i.

Values of burnout velocity and altitude for the maximum energy conditions discussed before are shown in Fig. 22. It logically follows that, since energy is a function of velocity and altitude, these curves are coincident in the same manner as the maximum energy curves at low burnout angles. At higher burnout angles, burnout velocity increases and burnout altitude decreases as n_i is increased.

Each representative trajectory tabulated in Table V is the nearest trajectory available to the overall maximum energy case for that particular n_i.

This is the optimum trajectory for the burnout angle listed only, and it cannot be said that it is the optimum trajectory for any other attitude reached before burnout. Naturally it is not applicable to a burnout angle lower than that listed. The question arises whether or not more energy is obtained by using the tabulated trajectory for the overall maximum energy case until the desired attitude is obtained, followed by constant attitude thrust until burnout, than by using the maximum energy trajectory for the burnout angle corresponding to the attitude desired. It seems that if the vehicle is above the denser atmosphere, the energy generated after constant attitude thrust is started would be about the same as that for the gravity turn. A constant attitude thrust program would give higher altitude with lower velocity than the gravity turn, although the actual difference between the two programs would depend upon the time of application of the constant attitude thrust program. If the vehicle reaches the desired attitude in the early tilt phase, before leaving the denser atmosphere, a constant attitude thrust program would involve lift loads and additional drag, but it would get the vehicle out of the sensible atmosphere sooner. In either case the non-linearity of the problem would require a separate computation for each situation.

CHAPTER 8

CONCLUSIONS

Determining the optimum powered flight trajectory for a large rocket powered vehicle is a complex problem, which is strongly influenced by the desired trajectory burnout angle and the rocket initial thrust-to-weight ratio. The burnout angle may be considered a design parameter for the booster trajectory, since different burnout angles are required for different missions. This paper shows that a combination of vertical flight time and initial tilt angle to give maximum energy at burnout can be determined for any desired burnout angle. There is, in addition, one value of burnout angle, which gives maximum burnout energy, for each value of initial acceleration. In this manner an optimum booster flight trajectory is available for any desired burnout angle.

Usually the vehicle with the higher initial acceleration will have the greater burnout energy. At low burnout angles, however, in the zero to ten degree range, values of burnout energy for a wide range of initial accelerations closely coincide. For low burnout angles, therefore, the initial acceleration of the vehicle is of little consequence with respect to maximum energy optimization. In fact, it can be said that a lower initial acceleration is preferable for low burnout angles, since the high lift load factors associated with high initial accelerations are avoided.

The time required to tilt the vehicle from the vertical to a point where the angle-of-attack is zero is also quite high for high acceleration vehicles. The procedure involving a relatively small initial tilt angle followed by a gravity turn to the desired burnout angle is no longer feasible with high initial accelerations, which leads to the conclusion that the tilt phase for high initial acceleration vehicles must be programmed in its entirety.

APPENDIX A

ATMOSPHERIC DATA

The atmospheric data used is based on the ARDC model atmosphere of 1959 as described in Ref. 3. In order to facilitate computer procedures the density ratio (ρ/ρ_o) and sonic speed data are treated in a simplified manner.

Utilizing the atmospheric density data of Ref. 3 a plot of the ratio of ρ/ρ_o is made extending from sea level to an altitude of 400,000 feet, as shown in Fig. 32. The resulting curve is divided into four segments which are accurately approximated by appropriate exponential functions. The resulting segments of the curve and respective describing exponential functions representing the density ratios are shown in Table VI.

Sonic speed is plotted versus altitude from sea level to an altitude of 400,000 feet as shown in Fig. 33. The curve results in a series of five straight line segments. Straight line functions are used to describe these segments of the curve. Table VI displays these functions and their respective areas of applicability.
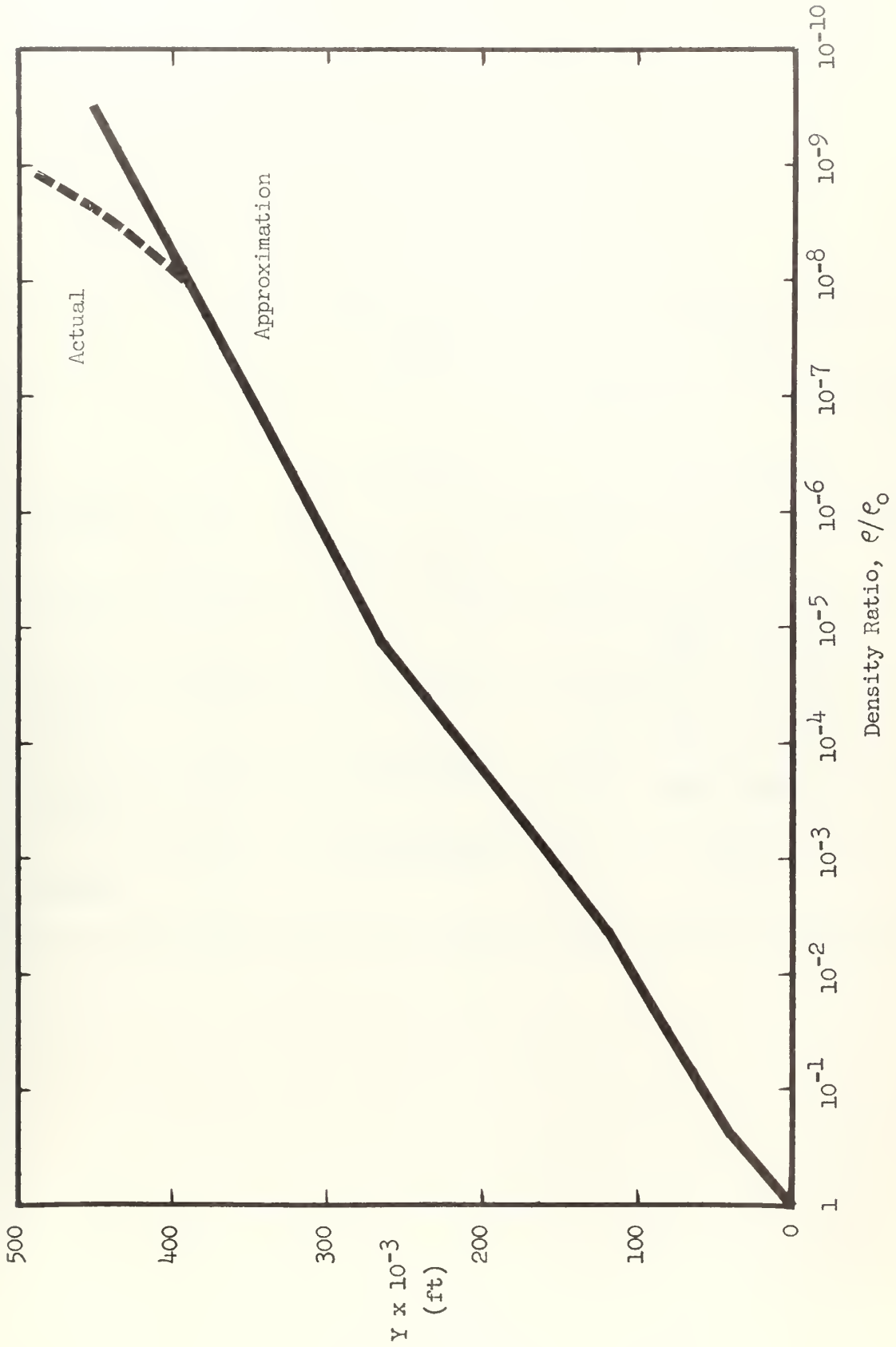
Fig. 32 Variation of density ratio with altitude.

TABLE VI

ATMOSPHERIC DATA APPROXIMATION FORMULAS

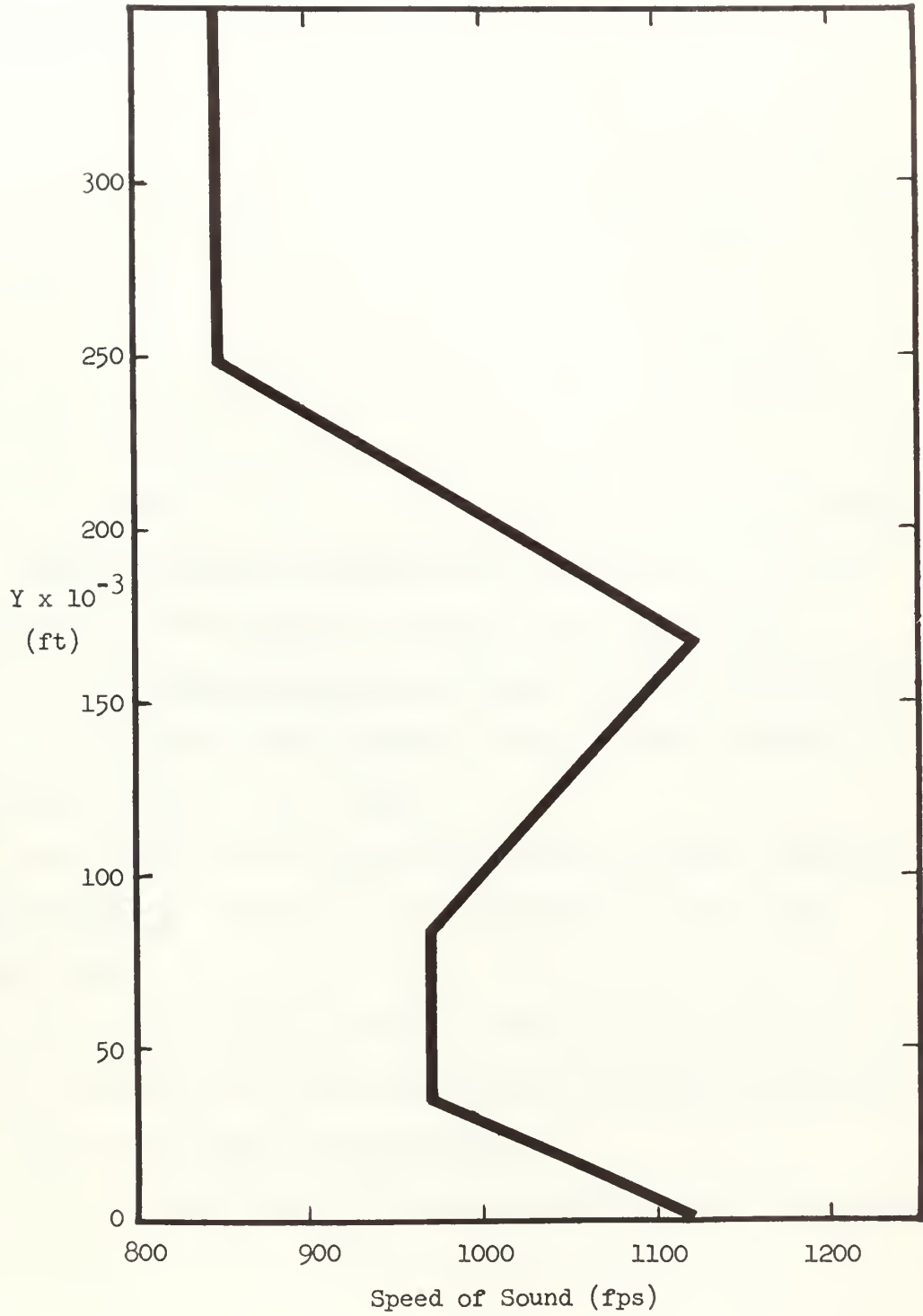| Altitude (ft)	Density Ratio ρ/ρ_o	Speed of Sound (fps)
0 36,800	$e^{-Y/32,000}$	1120-.00417 Y
82,500	1.65 $e^{-Y/20,800}$	968.08
120,000	1.65 $e^{-Y/20,800}$	813.78 .00187 Y
168,000	.51 $e^{-Y/25,200}$	813.78 .00187 Y
263,000	.51 $e^{-Y/25,200}$	1625-.00298 Y
450,000	77 $e^{-Y/17,000}$	846.5

Fig. 33   Variation of speed of sound with altitude.

REFERENCES

1. Prigge, J.S., Jr., Parsons, T., and Berman, L., A Digital Computer Study of the Powered Flight Trajectory of Long Range Ballistic Missiles, Report ARG-1, USAF 33(616)2392, 1956.

2. Traenkle, C.A., "Mechanics of the Power and Launching Phase for Missiles and Satellites", Wright Air Development Center Technical Report 58-579, September, 1958.

3. Minzer, R.A., Champion, K.S.W., Pond, H.L., "The ARDC Model Atmosphere 1959," Airforce Surveys in Geophysics No. 115, Geophysics Research Directorate, Air Force Cambridge Research Center, August 1959.

4. Sandorff, P.E., Orbital and Ballistic Flight, Technical Publications Group of the Instrumentation Laboratory, Massachusetts Institute of Technology, Cambridge, 1960, Chapter 3.

5. Fried, B.D., "Trajectory Optimization for Powered Flight," Chapter 4 in Space Technology, Seifert, H., ed., John Wiley and Sons, Inc., New York, 1959.

6. Hoult, C.P., GRD Research Notes No. 17, "The Approximate Analysis of Zero Lift Trajectories," August 1959, Geophysics Research Directorate AFCRC, ARDC, USAF, Bedford, Massachusetts.

7. Bryson, Ross, "Optimum Trajectories with Aerodynamic Drag," Jet Propulsion 28, 465, 1958.